Transportation Research Interdisciplinary Perspectives 28 (2024) 101289

Contents lists available at ScienceDirect

Transportation Research Interdisciplinary Perspectives

journal homepage: www.sciencedirect.com/journal/transportation-research-interdisciplinary-perspectives

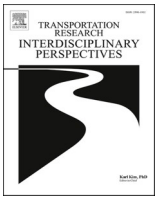

Optimizing travel costs of feeder-integrated public transport system: A methodology

Mysore Narasimhamurthy Sharath [a,f], Babak Mehran [a,*], Ahmed Ashraf [b], Susan Grant-Muller [c], Ed Manley [d,e]

[a] Urban Mobility and Transportation Informatics Group, Department of Civil Engineering, University of Manitoba, Winnipeg, Canada
[b] Department of Electrical and Computer Engineering, University of Manitoba, Winnipeg, Canada
[c] Institute for Transport Studies, University of Leeds, Leeds, United Kingdom
[d] School of Geography, University of Leeds, Leeds, United Kingdom
[e] Leeds Institute for Data Analytics, University of Leeds, Leeds, United Kingdom
[f] Department of Civil Engineering, Alliance University, Bengaluru, India

ARTICLE INFO

Keywords:
3-echelon vehicle routing
Multi-objective optimization
Fuzzy inference systems
Demand-responsive sustainable public transportation
Evolutionary algorithm

ABSTRACT

Canada, with a substantial contribution from the personal transport sector, is a major per capita greenhouse gas emitter. This study advocates a sustainable 3-echelon transportation system, integrating Public Transit (PuT) and demand-responsive transit (DRT) for door-to-door service. Electric autonomous DRT vehicles serve the first and third legs of travel, while the second leg relies on PuT. The goal is to identify routes for commuters simultaneously optimizing user, operator, and emission costs. A novel evolutionary algorithm, guided by fuzzy inference systems, optimizes travel costs. The algorithm is calibrated, and its performance is validated against benchmark instances. The proposed optimization framework demonstrates superior performance, achieving quick convergence even for large instances with over 5,000 billion possible routes. Near-optimal routing solutions for sizable scenarios with approximately 100 commuters, 250 PuT nodes, and 50 DRT vehicles can be computed within approximately 20 min.

1. Introduction

Canada emitted 16.44 tonnes of GHGs per capita in 2018, ranking among the world's highest (Ritchie et al., 2020). The transport sector contributes 27 % of total GHG emissions, with half coming from passenger transportation (Davis et al., 2018). Promoting Public Transit (PuT) is crucial to reduce emissions; but door-to-door service is unachievable, deterring certain commuters like older adults and those with mobility needs. Extreme weather events further discourage PuT usage. Thus, establishing door-to-door services is essential to minimize usage of personal vehicles. This study examines a 3-echelon transportation system to address this issue. Integrating PuT with ride-sharing is a promising alternative (Thao et al., 2021; Whitmore et al., 2022).

Electric Autonomous Demand-Responsive Transit Vehicles (AuDRTVs) acts as feeders for PuT, providing door-to-door service. PuT and AuDRTVs together reduce the costs of the door-to-door transportation system. User cost, operator cost, and emission cost of the 3-echelon transportation system are simultaneously optimized. As a result, the proposed system architecture is expected to be pocket-friendly, environment-friendly, and sustainable.

In the first echelon, a passenger travels from an origin (specified by the passenger) to a suitable PuT node (using AuDRT). In the second echelon, the passenger travels between two specified PuT nodes (using PuT). Finally, the passenger travels to the desired destination in the third echelon (using AuDRT). The three echelons involve three different vehicles; electric AuDRTVs in the first and third echelons (as feeders to PuT), and the mass PuT vehicles in the second echelon. AuDRTVs are assumed to start and terminate their trip at a *service station*. The route between the passenger's origin and destination involves all three echelons. The aim is to optimize the travel costs of this 3-echelon transportation system. Travel cost optimization is widely studied in the literature (Agatz et al., 2012; Rattanawai et al., 2024; Zhang et al., 2022). Despite being common, the three-echelon transportation system is seldom considered for cost optimization.

This study optimizes multiple travel costs of a multi-echelon transportation system. Evolutionary Algorithms (EA) are widely used for

* Corresponding author.
E-mail address: Babak.Mehran@umanitoba.ca (B. Mehran).

https://doi.org/10.1016/j.trip.2024.101289
Received 20 September 2024; Received in revised form 26 November 2024; Accepted 27 November 2024
Available online 7 December 2024

multi-objective optimization (Guo et al., 2022; Kabir et al., 2023). However, this study develops a novel methodology (which is termed F3E-MOGA, short for fuzzy-guided 3-echelon multi-objective genetic algorithm) utilizing fuzzy inference systems to guide the genetic operations of an EA to optimize a 3-echelon multi-objective transit system.

1.1. System architecture and solution representation

Fig. 1 depicts the three-echelon architecture. There are three categories of nodes in the network. The first is the 'Service Station' ($\mathbb{S}$), where the AuDRTVs originate, terminate, and undergo maintenance. Nodes corresponding to 'Passenger Origins' ($\mathbb{P}$) and 'Passenger Destinations' ($\mathbb{D}$) are the second type of nodes in the network. 'Public Transit' nodes ($\mathbb{R}$) constitute the third type of node.

A passenger's travel consists of three legs (echelons). In the first leg, AuDRTV-1 travels from a service station to the passenger's origin. After dropping off the passenger at a PuT node, AuDRTV-1 returns to a service station for maintenance. The second leg involves fixed-route, fixed-schedule PuT travel between specified nodes. While PuT can use electric vehicles, this study intentionally examines diesel engine vehicles due to their current prevalence and local emissions impact. In the third leg, AuDRTV-2 picks up the passenger from a PuT node, transports them to their destination, and returns to a service station. These three echelons are depicted in Fig. 1(a).

The system can also be represented with eight nodes, as shown in Fig. 1(b). Nodes 1, 4, 5, and 8 represent the service stations. Nodes 3 and 6 correspond to PuT nodes. Nodes 2 and 7 are the passenger's origin and desired destination, respectively. Such a representation of 3-echelon travel using eight nodes makes it possible to model the travel solution to a passenger demand using an eight-element vector, as depicted in Fig. 2(a).

In the EA, an eight-element vector is termed a 'chromosome'. Each element in a chromosome is a 'gene'. Every gene in a chromosome represents a node in the network. Fig. 2(a) furnishes route solution for multiple passengers as stacked chromosomes. Every gene has associated geo coordinates. Hence, it is possible to present the travel solution for each passenger in a cartesian plane. One such fictitious route solution for Passenger 2 is presented in Fig. 2(b).

Node Position	1	2	3	4	5	6	7	8
Node Type	$\mathbb{S}$	$\mathbb{P}$	$\mathbb{R}$	$\mathbb{S}$	$\mathbb{S}$	$\mathbb{R}$	$\mathbb{D}$	$\mathbb{S}$
Passenger 1	11	1	27	19	12	26	31	15
Passenger 2	18	2	24	15	19	30	32	16
Passenger 3	11	3	24	13	20	30	33	16
Passenger 4	17	4	23	11	14	23	34	16
Passenger 5	12	5	23	19	12	22	35	15
Passenger 6	15	6	22	12	19	29	36	14
Passenger 7	12	7	21	12	17	21	37	17
Passenger 8	13	8	25	20	18	28	38	18
Passenger 9	18	9	28	12	12	30	39	19
Passenger 10	13	10	28	14	12	28	40	14

(a)

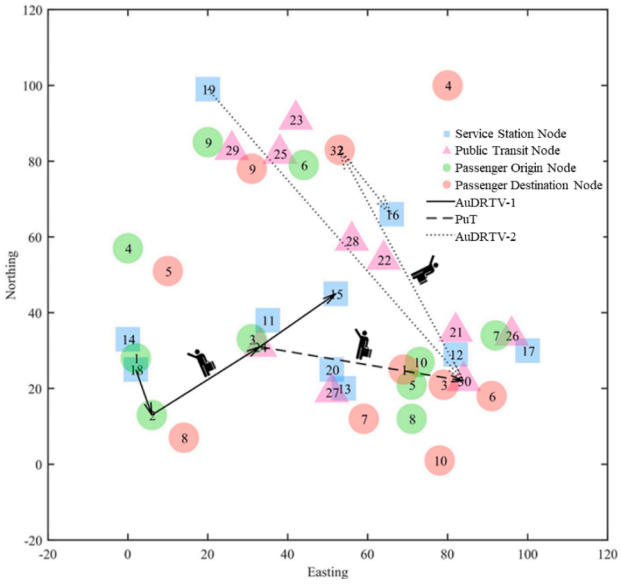

(b)

Fig. 2. (a) Chromosome representation and (b) route depiction for Passenger 2.

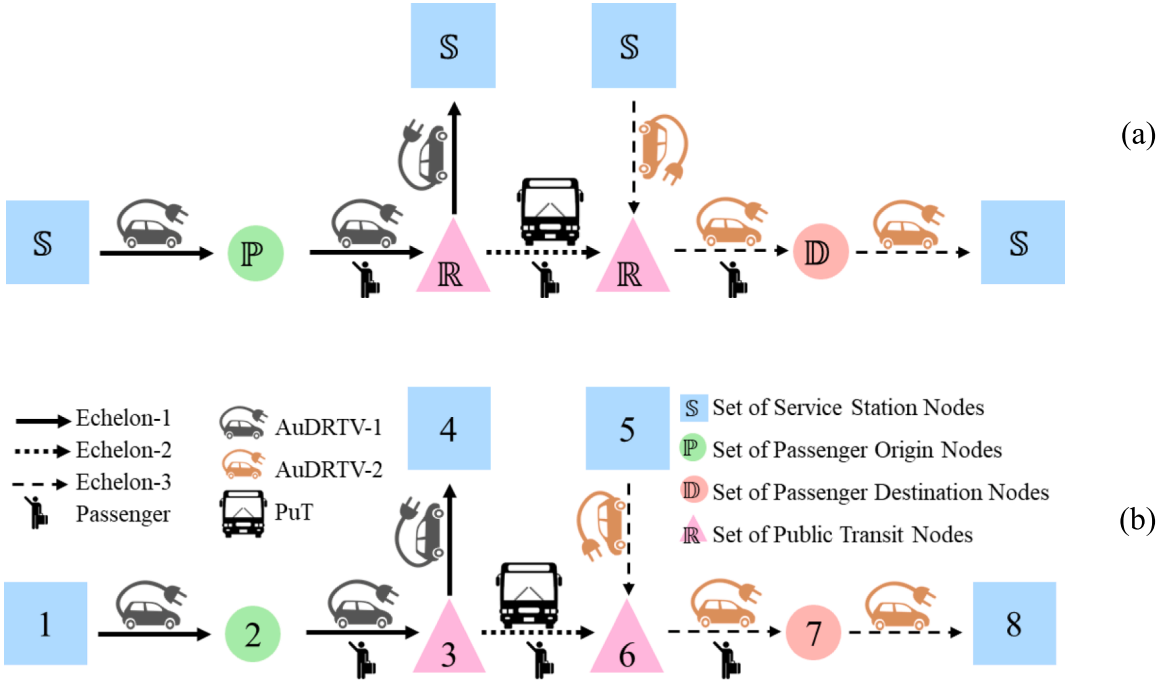

Fig. 1. (a) The three echelons of the proposed integrated system; (b) enumerated nodes.

1.2. The rationale behind 3-echelon system architecture

(i) Even though 2-echelon transit systems are well explored (Belgin et al., 2018; Dellaert et al., 2019), systems like supply chain and PuT commuting require three echelons for accurate modeling. Our study integrates DRT with PuT using a three-echelon model, reflecting real-world complexity and the need for comprehensive modeling.
(ii) Integrating DRT with PuT reduces passenger costs compared to standalone DRT systems, making door-to-door service feasible.
(iii) Simple modifications can convert the proposed 3-echelon system architecture into two or single echelon architectures.

This study confines itself to a 3-echelon system (with two transfers). The inherent ability to reduce the echelons by simple modifications is one of the main reasons for proposing the 3-echelon transit system in this study.

2. Literature review

2.1. Integration of evolutionary algorithms and fuzzy systems for solving vehicle routing problems

Vehicle routing is a popular research topic that has been widely and thoroughly researched for many decades (Braekers et al., 2016; Elshaer and Awad, 2020; Nickkar et al., 2022). The section is therefore limited to reviewing relevant and recent studies that have integrated any EA with fuzzy inference systems in solving vehicle routing problem.

Lau et al. (2009) employed fuzzy logic to dynamically control the crossover and mutation rates of several multi-objective EAs. They attempted to solve multi-commodity capacitated Vehicle Routing Problems (VRP). Nondominated sorting genetic algorithm with fuzzy-guided rates of genetic operations outperformed other EAs tested.

Cao and Lai (2010) used a fuzzy chance-constrained program to model the fuzziness in travel demands. They used a differential evolution algorithm to solve the open VRP with fuzzy demands. Feng and Liao (2014) used a fuzzy clustering approach for solving large-scale traveling salesman problems. They employed a table transform-based particle swarm optimization algorithm coupled with simulated annealing.

Conformance (or violation) of service time windows (preferred by passengers) is a measure of passenger satisfaction. But the boundaries between satisfactory levels are fuzzy. Hence, fuzzy inference systems are used to express passengers' satisfaction levels (Ghannadpour and Zarrabi, 2019). In a similar study, Ghannadpour et al. (2014) used fuzzy membership functions to express passengers' satisfaction based on their importance levels. They employed a multi-objective genetic algorithm to solve the dynamic VRP with fuzzy time windows.

Yan et al. (2020) recently solved a single objective 2-echelon VRP by integrating a fuzzy inference system with an EA. The second echelon routes are heuristically minimized, considering customer correlations. Fuzzy subsets of second echelon nodes are utilized.

Sometimes, knowing the relative importance of different objectives may be possible. Passengers may be able to prioritize (or provide relative importance) between the objectives (for example, when optimizing travel time and cost). In such cases, a solution from the non-dominated frontiers could be chosen to optimize more preferred objectives. However, the relative importance is fuzzy in nature. Hence, a method to express relative importance using fuzzy membership functions was provided (Shen et al., 2010).

Often in literature, a single-echelon variant of VRP is solved. The capability of FIS to achieve superior convergence is not exploited. The present study solves a challenging multi-objective 3-echelon variant of VRP. FISs govern the genetic operations of F3E-MOGA for superior convergence.

2.2. Relevant 3-echelon multi-objective problems

F3E-MOGA solution for each passenger would have three routes making it a 3-echelon system (see Fig. 1). 3-echelon VRPs are rarely addressed in the literature. Optimizing multi-echelon logistics supply chains (LSCs) is a problem like multi-echelon VRPs (Srivatsa Srinivas and Marathe, 2021). LSCs containing three levels (but termed 4-echelon systems in LSCs) may be similar to F3E-MOGA.

Multiple options are optimized in LSCs using approaches like EAs and integer programming models. Yet, the network size considered is relatively small. In contrast, the present study considers up to 100 customer nodes, 30 service station nodes, and 300 transit nodes. The large number of nodes in a network disproportionately increases the solution complexity. F3E-MOGA can solve much larger practical problems than existing studies.

2.3. Solving vehicle routing problem

Vehicle routing models are extensively used to optimize transportation networks. Passengers' commutes are often composed of multiple legs (or levels or echelons) of travel. Each leg of a trip may be served by a different travel mode (or vehicle). Assigning vehicles to passengers and deciding the travel routes while optimizing specific objectives is the essence of vehicle routing. Certain constraints are to be adhered to in the process. In the context of VRP involving passenger transportation, several objectives can be explored. Optimization of travel time, waiting time, and travel distances are widespread (Coindreau et al., 2019). Optimization of vehicle acquisition and operational costs is often performed (Alogdianakis and Dimitriou, 2023; Guo et al., 2019; Masmoudi et al., 2022).

With the advent of electric vehicles, objectives such as battery recharging and charging station setup costs are explored (Dimatulac et al., 2023; Hulagu and Celikoglu, 2022). Environmental cost, i.e., minimization of GHG emissions (fuel consumption), is a popular objective (Rezaei et al., 2022; Ye et al., 2022). Objectives like passengers' out-of-pocket cost and service quality (discomfort due to ride-sharing, passenger load factor, etc.) are seldom optimized in the literature (Aiko et al., 2018). Interested readers may refer to literature on VRP for a comprehensive classification, taxonomy, and state-of-the-art (Braekers et al., 2016; Díaz-Parra et al., 2014; Elshaer and Awad, 2020; Konstantakopoulos et al., 2020; Lin et al., 2014; Vidal et al., 2020).

Multi-echelon VRP is one of the variations of the VRP. Machine learning approaches for solving such problems are gaining popularity (Parvez Farazi et al., 2021). Several heuristics are being developed to solve large scale problems (Aloui et al., 2021). Each leg of travel constitutes an echelon of a transit system. 2-echelon VRPs are explored in the literature (Agárdi et al., 2021; Farajzadeh et al., 2020; Gayialis et al., 2019). 3-echelon transit systems are observed in the real world but are seldom modeled (Beheshtinia et al., 2021; Saragih et al., 2019). The focus of this study is on solving a 3-echelon multi-objective VRP. Vehicle routing in such an architecture requires making the following decisions (Please refer to Table 1 for notations used in this study):

(i) $\mathbb{S}-\mathbb{P}$ assignment in the first echelon
(ii) $\mathbb{P}-\mathbb{R}$ assignment in the first echelon
(iii) $\mathbb{R}-\mathbb{S}$ assignment in the first echelon
(iv) $\mathbb{R}-\mathbb{R}$ assignment in the second echelon
(v) $\mathbb{S}-\mathbb{R}$ assignment in the third echelon
(vi) $\mathbb{R}-\mathbb{D}$ assignment in the third echelon
(vii) $\mathbb{D}-\mathbb{S}$ assignment in the third echelon

The computation of the optimal path between a pair of nodes is a well-researched and challenging problem. This study assumes the availability of optimal paths (and the related travel costs) between pairs of origins and destinations at any given time. The emphasis is on solving

Table 1
Notations and descriptions.

Notation	Description
s	A service station with an available AuDRTV
s'	A service station without any available AuDRTV
$\mathbb{S}$	Set of all service stations with an available AuDRTV,$\mathbb{S} = \cup s$
$\mathbb{SS}$	Set of all service stations,$\mathbb{SS} = \mathbb{S} \cup s'$
p	A passenger origin
$\mathbb{P}$	Set of all passenger origins,$\mathbb{P} = \cup p$
m	Destination of a passenger
$\mathbb{D}$	Set of destinations;$\mathbb{D} = \cup m \forall p$
r	A PuT station
$\mathbb{R}$	Set of all PuT stations,$\mathbb{R} = \cup r$
$\mathbb{N}$	Set of all nodes;$\mathbb{N} = \{\mathbb{S}, \mathbb{P}, \mathbb{D}, \mathbb{R}\}$
ij	The shortest edge connecting origin node i and destination node j
d_{ij}^u	Travel distance for passenger u while traveling between nodes i and j
h_{ij}^u	Travel time for passenger u while traveling between nodes i and j

the problem of vehicle routing, passenger-vehicle assignment, and vehicle-service station assignment. User and operator costs are simultaneously optimized by employing a nondominated sorting EA. Four random genetic operators developed for F3E-MOGA prevent the solutions from getting stuck in local optima. Fuzzy-guided genetic operators in F3E-MOGA guarantee superior convergence.

2.4. Contributions and policy implications

2.4.1. Development of fuzzy-guided genetic operators

F3E-MOGA is developed by fusing FISs with an EA. Several random genetic operations are explicitly developed for the problem. Further, FISs guide genetic operations to increase the solution convergence rate. The concept of Neighborhood Score is introduced to improve the quality of emerging solutions. Besides improving the convergence rate, fuzzy guidance also yields superior convergence.

2.4.2. Solutions to multi-objective 3-echelon VRPs

3-echelon optimization is computationally challenging, and such complex problems are seldom solved in literature. The proposed F3E-MOGA can solve pragmatically large networks by simultaneously optimizing multiple objectives.

2.4.3. Benchmarking

Despite being common, 3-echelon transit systems are rarely explored. Hence, there does not exist any dataset with known optimal solutions. This poses a challenge in assessing the quality of F3E-MOGA. This study generated several instances (with small complexities) and optimized them with exhaustive exploration techniques. These optimal solutions are used as benchmarking instances against which the quality of F3E-MOGA is assessed. Benchmarking instances and the optimal solutions would be furnished upon request.

2.4.4. Policy implications

The developed solution methodology provides policymakers with a tool to optimize travel costs in real-world multi-echelon systems, such as logistics supply chains and integrated public transit networks. This approach addresses a critical gap, as methodologies for modeling and optimizing large-scale 3-echelon systems are scarce.

From a policy perspective, the methodology has significant environmental and economic implications. By optimizing resource utilization, it can guide policies aimed at reducing carbon emissions and operational costs. For example, governments can adopt this methodology to develop sustainable transport policies that minimize environmental impact while maximizing economic efficiency.

In the context of public transit, the methodology can inform policies to improve service accessibility, particularly for vulnerable populations. This is crucial in ensuring equitable public transit availability, especially during adverse weather conditions or other disruptions. Policymakers can use these insights to prioritize investments in transit infrastructure and optimize transit routes for greater inclusivity and resilience.

3. Problem description

A 3-echelon architecture is envisioned to promote PuT usage with door-to-door service. Such a transportation system's travel costs (operator, user and emission costs) are optimized by fusing FISs and an EA.

3.1. Network representation and notations

The 3-echelon transit network is modeled as a graph consisting of nodes and edges. The cost of traveling along a road link is modeled by the corresponding edge cost. Nodes indicate the locations of passengers' origins, destinations, service stations, and transit stops. Let $G = (\mathbb{N}, E)$ represent a road network as a graph with nodes $\mathbb{N}$ and edges E. G is a directed and weighted graph, which permits a comprehensive representation of an actual road network. There can be several origins, destinations, and transfer points in a transit network, all of which can be represented as nodes. Edges between any two nodes represent optimal AuDRTV routes or PuT routes. Table 1 describes the notations used in this study.

3.2. Optimization model

Travel for each passenger along the three echelons results in three types of costs. User Cost (UC) is the cost borne by the passenger; Operator Cost (OC) is the cost incurred by the transit operator; Emission Cost (EC) is the cost of local emissions. These three costs are conflicting in nature. Simultaneous minimization of these costs is thus a major challenge.

The monetary values of these objectives can be computed as:

$$f_1 = \text{minimize}UC = \sum_{\forall u}\left\{\left[\beta_0 + \beta_1 \times \left(d_{pr}^u + d_{rm}^u\right)\right] + f_{rr}^u \times x_{rr}^u\right\} \forall p \in \mathbb{P}, r \in \mathbb{R}, m \in \mathbb{D} \tag{1}$$

$$f_2 = \text{minimize}OC = \sum_{\forall u}\left\{\beta_1 \times \left(d_{sp}^u + d_{rs}^u + d_{sr}^u + d_{ms}^u\right) + \alpha \times h_{rr}^u\right\} \forall p \in P, r \in R, m \in D, s \in \mathbb{S} \tag{2}$$

$$f_3 = \text{minimize}EC = \sum_{\forall u} \beta_2 \times d_{rr}^u \forall r \in R \tag{3}$$

Equation (1) minimizes the UC. The suffixes p, r and m indicate the passenger origin node, transit node and passenger destination node respectively. Hence, the travel between p and r is in the first echelon, while the travel from r to m is the final leg of travel, both of which are served by the demand-responsive transit vehicles, similar to taxis. The operating cost of taxi services is proportional to the vehicle distance travelled (Mehran et al., 2020). Hence, the cost of traveling in the first and third echelons is computed as a function of the distance travelled (β_0 is the minimum fixed cost per trip of AuDRTVs and β_1 is the cost of traveling unit distance).

The travel between two PuT nodes (i.e., rr) is served by PuT buses. As per Mehran et al. (2020), the operating cost of the second echelon (PuT) can be estimated as a function of total vehicle hourly usage (α is the hourly cost of operating a vehicle per passenger). AuDRTV would be occupied by passengers while traveling between nodes $p\&r$ and $r\&m$ $\forall$ $p \in \mathbb{P}, r \in \mathbb{R}, m \in \mathbb{D}$. Further, there would be PuT usage fare, $f_{rr} \forall r \in \mathbb{R}$, (taken as C$3 in this study). These costs for user u, constitute the user cost, as given in Equation (1).

Equation (2) minimizes the OC. No passenger would be on board AuDRTVs during the travel between the following node pairs: $s\,\&\,p$, $r\,\&\,s$,

s & r, and m & s $\forall p \in P$, $r \in R$, $m \in D$, and $s \in \mathbb{S}$. The operator will bear these travel costs and the cost of operating PuT. Total operator cost is determined as in Equation (2).

AuDRTVs are considered battery autonomous vehicles, which originate and terminate at a service station. As such, AuDRTVs do not contribute to local emissions. The second echelon travel is facilitated by public transit, which is assumed to be served by conventional diesel powered 12 m long buses with passenger capacity of 70. The emission cost of such a vehicle is computed based on the distance travelled (1.254C$/km) (Barraza and Estrada, 2021). The total emission cost of all three echelons is obtained as in Equation (3).

The values of the coefficients ($\beta_0 = \$4$ and $\beta_1 = 1.81$ C$/km) are adopted from Mehran et al. (2020). A value of $\alpha =$ C$8 per hour per passenger is chosen in this study. Emission cost coefficient $\beta_2 = 1.254$ C$/km is used based on the literature (Barraza and Estrada, 2021; Querini et al., 2011). Appropriate values for the coefficients α and β may be chosen during adoption of the methodology. The choice of α and β will not necessiate recalibration of the model parameters as normalized units are used during calibration (Section 4.2).

Further, time spent by a passenger at a PuT node and slack time of the AuDRTVs may also be considered apart from the edge costs. However, the waiting time of vehicles (that are yet to be assigned a passenger) at the service stations is not a significant concern as the time may be utilized for recharging the batteries and maintaining/servicing the AuDRTVs. Further, PuT is considered reliable and frequent, implying that the waiting periods for passengers at PuT nodes are nominal.

Proof of concept is the primary goal of this study, hence there are only three objectives. Other objectives like fuel consumption, and service levels can be easily included. F3E-MOGA can easily handle multiple objectives.

4. Solution methodology

The three objectives used may be conflicting, and it is impossible to prioritize between them. It is also impractical to form a utility function including all the objectives, i.e., converting the multi-objective optimization problem into a single-objective optimization problem. Hence, a well-established multi-objective Pareto optimization approach using an EA (Deb et al., 2002) is used. Moreover, a Fuzzy inference system is integrated with the EA to guide the genetic operations and ensure superior convergence. Fig. 3 furnishes an overview of the proposed EA framework, emphasizing the development of custom-built random and fuzzy-guided genetic operators.

The locations of every node $n \subset \mathbb{N}$ and the travel demand for every passenger $p \subset \mathbb{P}$ would be known. A DRT operator would also have information about the availability of AuDRTVs at different service stations $s \subset \mathbb{S}$. Knowing this information, the initial solution is randomly generated. In the EA, routes for all passengers (stack of chromosomes (as shown in Fig. 2(a)) is termed a 'member'. Several such members constitute a 'population'. Detailed description of EA is provided in the Annexure C for the purpose of brevity; however, the methodology for parameter calibration, fuzzy inference systems and fuzzy guided genetic operations are described in this section.

4.1. Methodology for parameter calibration

The study employed fuzzy inference systems and developed several genetic operators. Therefore, multiple parameters are used (see Table 2). Two parameters are used to represent the shape of the membership functions, while 17 other parameters indicate the probabilities of performing genetic operations. Two more parameters are used to identify a

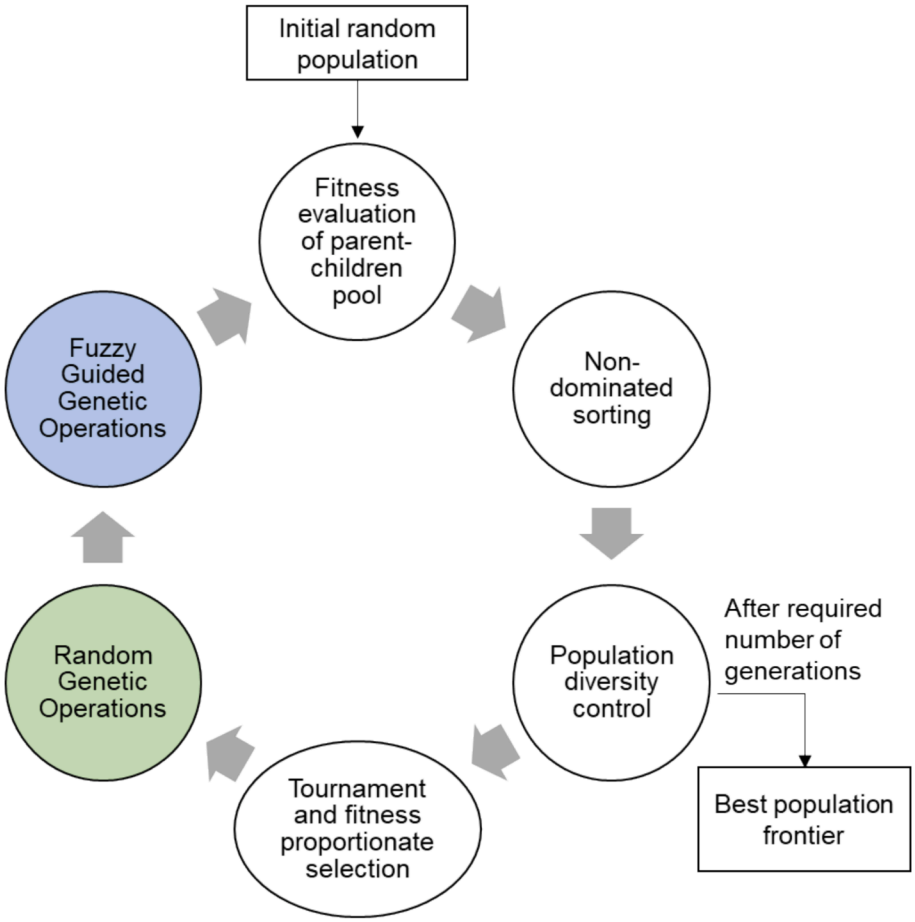

Fig. 3. Framework of the EA highlighting research contributions.

Table 2
Model parameters that are calibrated in the present study.

Sl No	Parameters	Level 1	Level 2	Level 3	Level 4	Calibrated Level
1	*SSX*	0	0.033	0.067	0.1	0.033
2	*PasRX*	0.1	0.167	0.233	0.3	0.233
3	*TNX*	0	0.033	0.067	0.1	0.100
4	*ParRX*	0	0.033	0.067	0.1	0.000
5	$FGGO_{12}$	0	0.033	0.067	0.1	0.033
6	$FGGO_{15}$	0	0.033	0.067	0.1	0.000
7	$FGGO_{23}$	0	0.033	0.067	0.1	0.033
8	$FGGO_{26}$	0	0.033	0.067	0.1	0.067
9	$FGGO_{36}$	0.1	0.167	0.233	0.3	0.300
10	$FGGO_{37}$	0	0.033	0.067	0.1	0.067
11	$FGGO_{45}$	0.1	0.167	0.233	0.3	0.300
12	$FGGO_{46}$	0	0.033	0.067	0.1	0.000
13	$FGGO_{47}$	0	0.033	0.067	0.1	0.033
14	$FGGO_{34}$	0.1	0.167	0.233	0.3	0.300
15	$FGGO_{56}$	0	0.033	0.067	0.1	0.067
16	$FGGO_{67}$	0	0.033	0.067	0.1	0.033
17	$FGGO_{78}$	0	0.033	0.067	0.1	0.000
18	α	5	10	15	20	10
19	β	3	5.333	7.667	10	3
20	PopSize	100	200	300	500	500
21	MinGenerations	100	200	300	400	300

suitable population size and the minimum number of generations. The list of parameters is presented in Section 5. Fig. 4 provides the procedure used for the calibration of the model parameters.

With 21 parameters and just four levels per parameter, an exhaustive exploration approach would result in 4^{21} ($\approx 4.4 \times 10^{12}$) unique combinations of parameters. It is impossible to explore so many combinations. Also, it is not prudent to sequentially calibrate the parameters considering one at a time. Such sequential calibration ignores the nonlinear correlation between the parameters. Hence, the fractional factorial experimental design approach proposed by Taguchi is used for simultaneously calibrating the model parameters (Abhang and Hameedullah, 2012; Sharath and Velaga, 2020; Taguchi et al., 2005). Taguchi's approach shortlists the unique parameter combinations for simultaneous calibration. Using L64b orthogonal array, the number of unique parameter combinations reduces to 64.

Parameters are optimal if the F3E-MOGA determined solution frontiers are similar to Pareto optimal frontier. Inverted Generational Distance (IGD) and Maximum Spread (λ) are the two popular indicators used to assess the quality of the solutions obtained from F3E-MOGA (Equations (4) and (5)).

$$IGD = \frac{1}{|\mathscr{F}^*|}\sqrt{\sum_{\forall k}(d_k)^2} \tag{4a}$$

$$d_k = min\sqrt{\sum_{\forall m,i}\left(f_{m,i} - f^*_{m,k}\right)^2} \tag{4b}$$

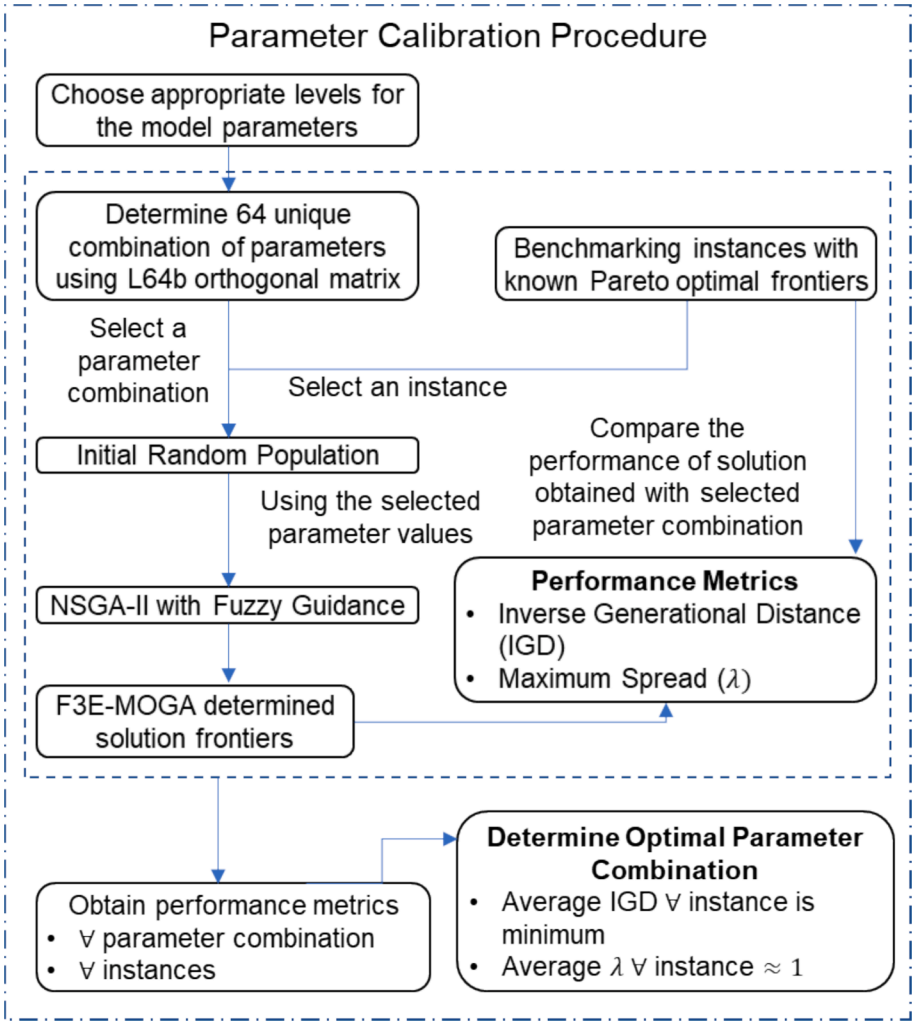

Fig. 4. Methodology used for calibration of model parameters.

$$\lambda = \sqrt{\frac{1}{M}\sum_{m=1}^{M}\left(\frac{f_m^{max} - f_m^{min}}{f_m^{*max} - f_m^{*min}}\right)^2} \quad (5)$$

where, $\mathscr{F}^*$ and $\mathscr{F}$ respectively are the Pareto optimal frontier and best frontier determined by F3E-MOGA;

$f_{m,k}^*$ is the m^{th} objective function value of k^{th} member of $\mathscr{F}^*$;
$f_{m,i}$ is the m^{th} objective function value of i^{th} member of $\mathscr{F}$;
f_m^{*max} and f_m^{*min} respectively are maximum and minimum value of m^{th} objective function in $\mathscr{F}^*$;
f_m^{max} and f_m^{min} respectively are maximum and minimum value of m^{th} objective function in $\mathscr{F}$;
M is the total number of objective functions.

Smaller IGD values indicate desirable convergence and diversity of $\mathscr{F}$ (Tian et al., 2016). The departure of λ from 1 indicates lack of uniform spread of the solution in $\mathscr{F}$. The method employed for calibrating the model parameters utilizing IGD and λ is presented in Fig. 4.

L64b orthogonal array permits 4 levels for each of the 21 parameters to be calibrated. Initially, appropriate levels for all the parameters are decided (this step is the trial-and-error method). Thus, 64 unique combinations of the parameters are generated. The study uses 11 benchmarking instances with known optimal solution frontier, $\mathscr{F}^*$, for each instance. Each of these instances is solved by F3E-MOGA using different parameter combinations. This process results in 64 solution frontiers, $\mathscr{F}$, for each instance. $\mathscr{F}^*$ and $\mathscr{F}$ are compared to compute IGD and λ, and the results are presented in Fig. 5 and Fig. 6. 95th percentile IGD and λ values during Taguchi tirals are $8.31 and 0.84. Only top 5 percentile values are shown in the dark shade. From the figures, it is evident that parameter combination 25 results in high-quality IGD and λ. Hence, such specific parameter combination is considered optimal. Detailed results are presented in Section 5.

Genetic operations are guided by a fuzzy inference system. The development of genetic operators is one of the significant contributions. Hence, Sections 4.3 and Annexure B are dedicated to describing them. Section 5 is dedicated to model calibration results, while Section 6 presents the results of solving large problem instances.

4.2. Fuzzy inference system and neighborhood score computation

4.2.1. Desired characteristics of a route solution

Good (near-optimal) routes may be assumed to have specific characteristics. Based on the intuition and general understanding of the transit system, desired characteristics of a route (for the network architecture considered) are conceived. The inherent assumption is that an optimal solution would also exhibit desired characteristics. The desired characteristics of a route are formulated as spatial (distance) and temporal (travel time) separations between the nodes.

For example, Nodes 1 and 2 in Fig. 7 represent the assignment of a service station to a passenger. Serving a passenger from a nearer service station appears preferable. Hence, the desired character between nodes 1 and 2 would be to have a smaller spatial and temporal separation.

Another contrasting example can be provided by considering the separation between nodes 4 and 5 in Fig. 7. Node 4 is the terminal service station of AuDRTV-1, and Node 5 is the origin service station of AuDRTV-2. If these two nodes are closer (assume overlap), the travel between PuT nodes 3 and 6 becomes redundant. Hence, a larger separation between nodes 4 and 5 is desired.

Similarly, it is possible to arrive at the desired characteristics (separations) of different node pairs. Smaller (spatial and temporal) separation is better for the following node pairs: 1&2, 2&3, 3&4, 5&6, 6&7, and 7&8. In contrast, a larger separation is preferred for the following node pairs: 1&5, 2&6, 3&6, 3&7, 4&5, 4&6, and 4&7. A pair of nodes is 'desirable' in the solution if it exhibits the desired separation characteristics. The optimal (or near-optimal) route would be a combination of desirable node pairs.

The terms like 'large separation', 'small separation', and 'good pairs' used to describe the routes' desired characteristics are qualitative and fuzzy. But a fuzzy inference formulation would permit quantifying these desired qualities/ characters. Thus, a fuzzy inference system is adopted.

4.2.2. Fuzzy inference systems for guiding genetic operations

A 2-input, one-output Sugeno fuzzy inference system is used in this study. Spatial separation (travel distance) and temporal separation (travel time) between a pair of nodes are the two input variables. The output is a Neighborhood Score (NS), which is a scalar quantity indicating the suitability of a node to be a neighbor to another (in the node

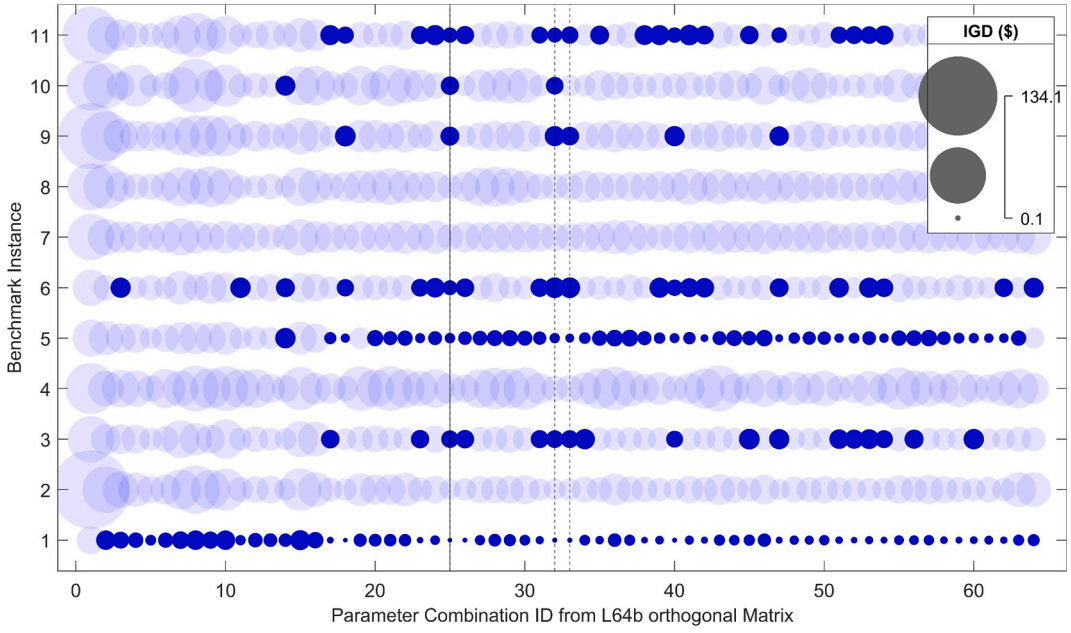

Fig. 5. Inverted generational distances. IGDs (averaged over 11 instances) for parameter combinations 25, 32 and 33 are $8.31, $8.5, and $9.17 respectively. The best combination ID (average IGD closest to 0) is shown with a solid line, while dashed lines indicate the combinations resulting in the top 5 percentile IGD values.

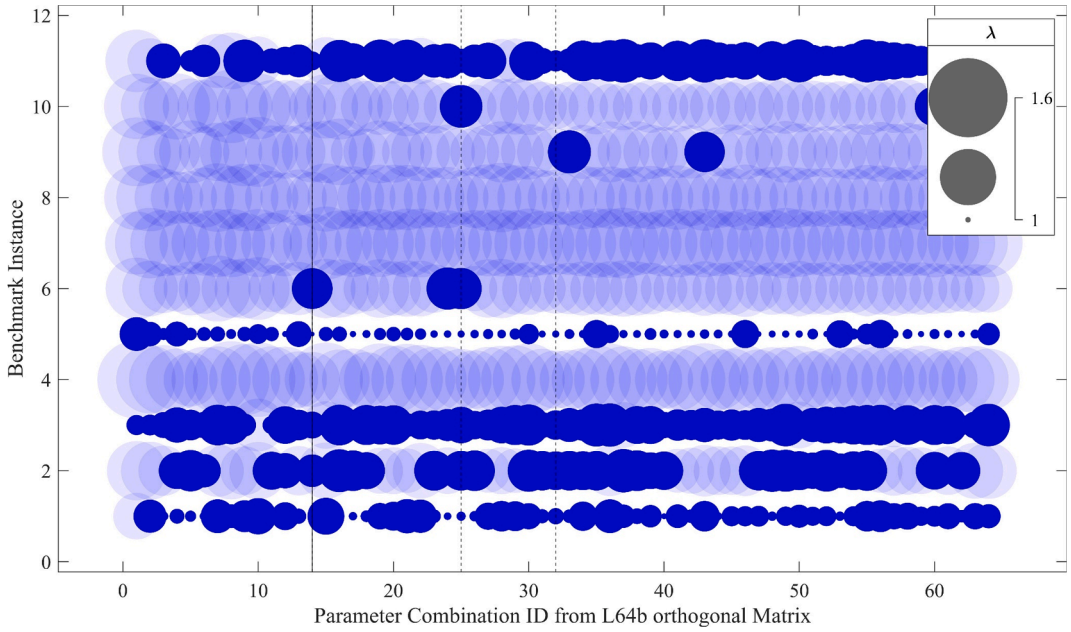

Fig. 6. Maximum spread, $\lambda.\lambda$ (averaged over 11 instances) for parameter combinations 14, 25 and 32 are 0.84, 0.831, and 0.83 respectively. The best combination ID (average λ closest to unity) is shown with a solid line, while dashed lines indicate the combinations resulting in the top 5 percentile λ values.

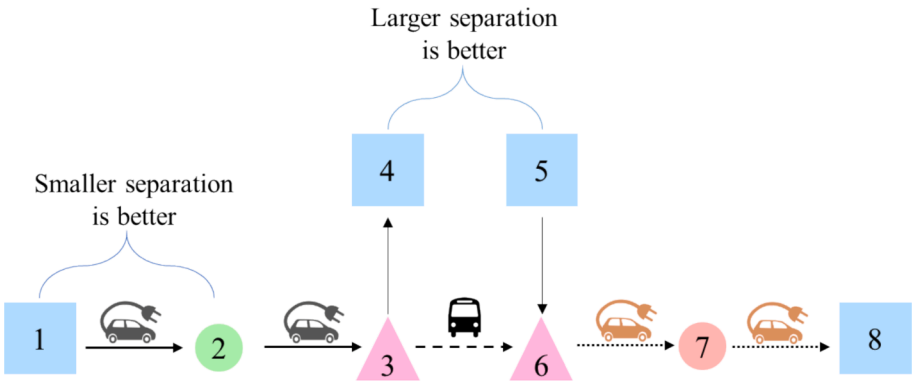

Fig. 7. Desired characteristics between node pairs 1–2 and 4–5.

pair).

Desirable node pairs (ideal neighbor to a node) are identified by computing NSs. The one with the largest NS is considered an ideal neighbor to a subject node among all possible neighboring nodes.

Three fuzzy membership functions are used to describe the (spatial and temporal) separations, as depicted in Fig. 8. The x-axis presents the scaled spatial or temporal proximity on a scale of 0 to 100. The separation can be converted into the actual distance or time units by choosing an appropriate scale factor. The scaling of the x-axis is necessary to avoid re-calibration of the parameters of the membership functions for different networks (of sizes and characteristics). Scaled membership functions could be used for various transit networks without re-calibrating parameters, making them network invariant. It is to be noted here that the scale factors are not dimensionless quantities. The spatial and temporal separation scale factors are determined as provided in Equations (6) and (7).

$$SF_{Distance} = \frac{Longesttraveldistanceintheconsideredtransitnetwork}{100} \tag{6}$$

$$SF_{Time} = \frac{Longesttraveltimeintheconsideredtransitnetwork}{100} \tag{7}$$

The elements of the fuzzy subset associated with 'Spatial Separation' are 'Small', 'Medium' and 'Large'. The same fuzzy subset is also used to represent 'Temporal Separation'. The elements of fuzzy subset attributed to NSs are 'Bad', 'Fair', and 'Good'.

A Z-shaped membership function is used to formulate 'Small' separation as shown in Equation (8). 'Large' separation is described using an S-Shaped membership function provided in Equation (9). Both of these membership functions have two parameters, α and b. However, if $b = SF \times 100 - \alpha$, the symmetry of membership function would be preserved.

$$f(x;\alpha,b) = \begin{cases} 1, x \le \alpha \\ 1 - 2\left(\frac{x-\alpha}{b-\alpha}\right)^2, \alpha \le x \le \frac{\alpha+b}{2} \\ 2\left(\frac{x-b}{b-\alpha}\right)^2, \frac{\alpha+b}{2} \le x \le b \\ 0, Otherwise \end{cases} \tag{8}$$

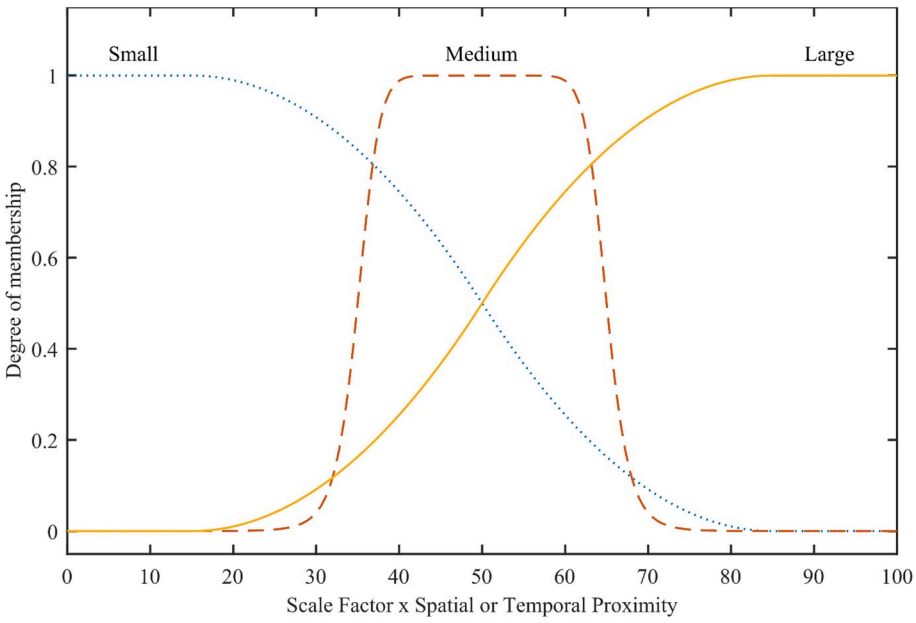

Fig. 8. Input membership functions.

$$f(x;\alpha,b)=\begin{cases}0, x\le\alpha\\ 2\left(\frac{x-b}{b-\alpha}\right)^2, \frac{\alpha+b}{2}\le x\le b\\ 1-2\left(\frac{x-\alpha}{b-\alpha}\right)^2, \alpha\le x\le\frac{\alpha+b}{2}\\ 1, \textit{Otherwise}\end{cases} \tag{9}$$

The third membership function for 'Medium' separation is described using a generalized bell-shaped membership function as in Equation (10). This membership function has three parameters, α, β and c. If $\alpha = SF\times\ a$, and $c = 50$, then the membership function would be symmetrical.

$$f(x;\alpha,\beta,c)=\frac{1}{1+\left|\frac{x-c}{\alpha}\right|^{2\beta}} \tag{10}$$

Hence, from Equations (8), (9), and (10), α and β are the only two parameters of the three membership functions to be calibrated. The other parameters (a, b, and c) are computed to preserve the symmetry of the membership functions and are functions of α as shown in Equation (11).

$$a=\frac{\alpha}{SF} \tag{11a}$$

$$b=SF\times 100-\alpha \tag{11b}$$

$$c=50 \tag{11c}$$

Constant output membership functions are used to describe NSs. A 'bad' NS is when it is 10; 'fair' when it is 50; and 'good' when it is 90.

4.2.3. *Knowledge-based fuzzy rules*

Several knowledge-based fuzzy rules are used to compute NS. Early in this Section, it is explained that separation (spatial and temporal) between node pairs is an essential characteristic of a solution (route). The solution tends to be optimal (or near-optimal) if the following fuzzy rules are satisfied.

4.2.3.1. Smaller separation is preferred. A smaller spatial and temporal separation between the following node pairs is preferred: 1&2, 2&3, 3&4, 5&6, 6&7, and 7&8. The solution tends to be near-optimal when the following fuzzy rules are satisfied:

11: If 'Spatial Proximity' is **Small** AND 'Temporal Proximity' is **Small**, THEN 'Neighborhood Score' is **Good**
21: If 'Spatial Proximity' is **Large** OR 'Temporal Proximity' is **Large**, THEN 'Neighborhood Score' is **Bad**
31: If 'Spatial Proximity' is Medium AND 'Temporal Proximity' is **Medium**, THEN 'Neighborhood Score' is **Bad**
41: If 'Spatial Proximity' is **Small** AND 'Temporal Proximity' is **Medium**, THEN 'Neighborhood Score' is **Fair**
51: If 'Spatial Proximity' is **Medium** AND 'Temporal Proximity' is **Small**, THEN 'Neighborhood Score' is **Fair**

4.2.3.2. Larger separation is preferred. In contrast, larger spatial and temporal separations are desired between the following node pairs: 1&5, 2&6, 3&6, 3&7, 4&5, 4&6, and 4&7. If the node pairs satisfy the below fuzzy rules, the solution tends to be near-optimal.

61: If 'Spatial Proximity' is **Large** AND 'Temporal Proximity' is **Large**, THEN 'Neighborhood Score' is **Good**
71: If 'Spatial Proximity' is **Small** OR 'Temporal Proximity' is **Small**, THEN 'Neighborhood Score' is **Bad**
81: If 'Spatial Proximity' is **Medium** AND 'Temporal Proximity' is **Medium**, THEN 'Neighborhood Score' is **Bad**
91: If 'Spatial Proximity' is **Medium** AND 'Temporal Proximity' is **Large**, THEN 'Neighborhood Score' is **Fair**
101: If 'Spatial Proximity' is **Large** AND 'Temporal Proximity' is **Medium**, THEN 'Neighborhood Score' is **Fair**

Fig. 9 provides the framework of the developed methodology to compute NSs. The spatial and temporal separations would be known for a given node pair. Knowing the separations, their corresponding membership values for different fuzzy subsets are computed. Fuzzy rules are then evaluated to obtain NS. α and β are the two parameters to be calibrated to compute NSs appropriately. The process of calibrating α and β is detailed in Section 5.

4.3. *Fuzzy-guided genetic operations*

NS between a pair of nodes is assumed to indicate the chance of

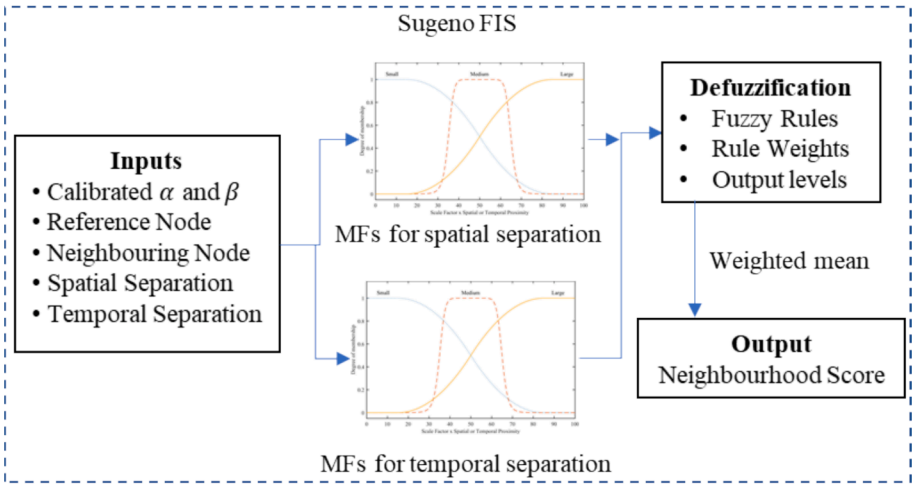

Fig. 9. Fuzzy inference system used for computation of Neighborhood Scores.

encountering that pair in the optimal route. Therefore, node pairs constituting smaller NSs are replaced with the node pairs that constitute larger NSs.

Consider a fictitious example, as shown in Fig. 10. $\mathbb{S} = \{11, 12, 13, 14, 15, 16, 17, 18, 19, 20\}$ form the set of all service stations. A randomly chosen passenger $p = 5 \subset \mathbb{P}$ could be served by any of the service stations belonging to $\mathbb{S}$. Hence, every member of $\mathbb{S}$ is a potential neighbor of $p = 5$. The most appropriate neighbor would be the one with the largest NS. The originally assigned service station $s = 12 \subset \mathbb{S}$ has a NS of 56. However, if the service station $s = 19$ is assigned to passenger $p = 5$, the resulting NS is 85, which is greater than 56. Hence, it would be desirable to serve passenger $p = 5$ from service station $s = 19$.

Instead of randomly determining the node pairs (assigning a service station to a passenger in the above example), NS (derived from a fuzzy inference system) can be used to determine the node pairs. Such guidance (heuristics), used in the form of genetic operators, can increase the convergence rate.

The mechanism mentioned above guides genetic operations between several node pairs. The 13 node pairs identified are 1&2, 2&3, 3&4, 5&6, 6&7, 7&8, 1&5, 2&6, 3&6, 3&7, 4&5, 4&6, and 4&7. Correspondingly, 13 probabilities of performing the genetic operations are to be calibrated. The process of calibrating the 13 parameters is described in Section 4.1.

5. Calibration and benchmarking

The present study has a total of 21 parameters that needs calibration. Using a single problem instance for calibration casts doubts about the transferability of the model. Hence, 11 instances were used for the calibration of the parameters (the procedure for creating benchmarking instances and the characteristics of benchmarking instances are detailed respectively in Annexures A and D). Based on the procedure described in the previous Section, the parameters are calibrated. Table 2 lists the model parameters, their corresponding exploration levels, and the

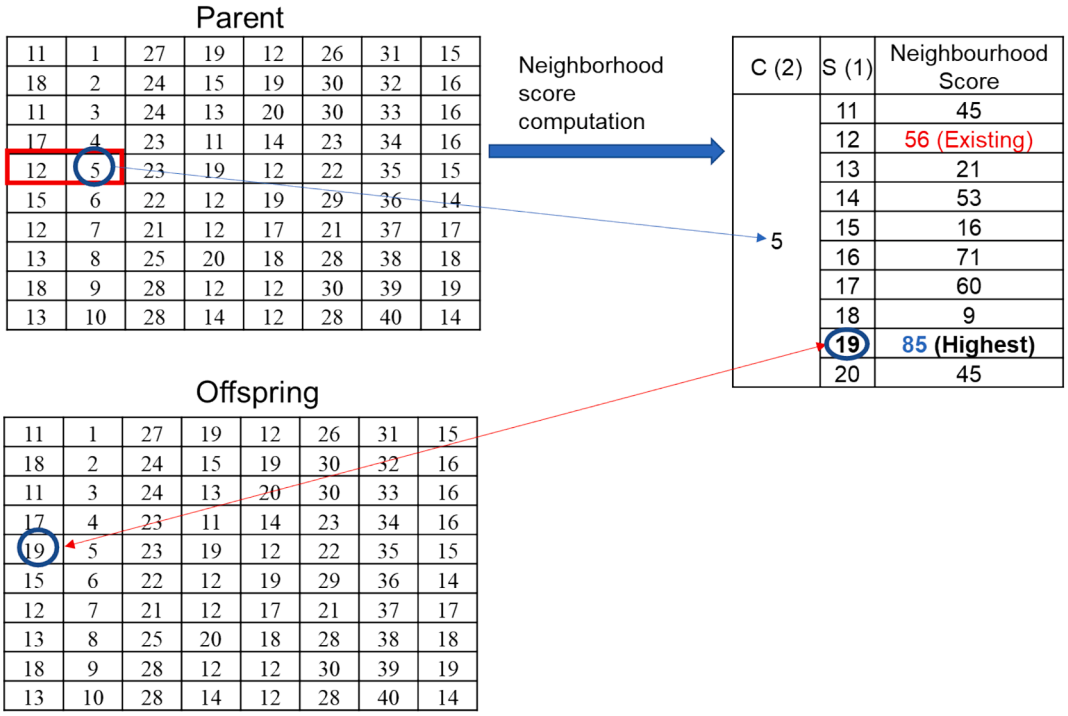

Fig. 10. An example of fuzzy-guided genetic operation between nodes 1 and 2.

calibrated (ideal) levels. Fig. 11(a) and (b) respectively depict the NS when (i) smaller spatial and temporal separations are better and (ii) larger spatial and temporal separations are better. Calibrated α and β are used to generate Fig. 11.

Pareto optimal solution frontier for 11 instances is determined by exhaustive exploration. The total number of nodes in these instances varied between 20 and 50, as presented in Table D.1. Further, the benchmark instances were solved by F3E-MOGA (using the calibrated parameters). The resulting solution frontiers are presented in Fig D.1(b), along with the Pareto optimal solution frontier Fig D.1(a). It can be observed that the F3E-MOGA determined frontier is very similar to the Pareto-optimal frontier, and the solutions appear to be well distributed along the Pareto frontier. Violin plots in Fig. D.2 (a, b and c) depict the distribution of (i) average operator cost, (ii) average user cost, and (iii) average emission cost in the solution frontier. The evidence from Fig. D.2 suggests that the best solution frontier determined by F3E-MOGA is similar to that of the Pareto optimal frontier (for all the benchmarking instances).

The distribution of the three costs in the best frontier as determined by F3E-MOGA closely resembles the distribution of costs in the Pareto optimal solutions across all benchmarking instances and objectives. This is a desired characteristic of any calibrated optimization algorithm. This suggests that the calibration of parameters of F3E-MOGA is appropriate.

6. Validation: Solving large problem instances

F3E-MOGA is benchmarked using 11 instances where $\Omega \leq 5 \times 10^6$. However, 20 larger instances are solved to exhibit the effectiveness of F3E-MOGA. The characteristics of the validation dataset are presented in Table D.2. The number of unique routing solutions in the dataset, Ω, ranges from 2 billion to 5,062 billion. For such an enormous value of Ω, it is impossible to compute the optimal frontier by an exhaustive search approach. F3E-MOGA is expected (and equipped) to determine a near-optimal solution quickly.

Fig. 12 furnishes the distributions of (i) average operator cost, (ii) average user cost, and (iii) average emission cost of best frontier of the large instances. The mean operator cost per passenger in the large instances is about $50 per passenger, compared to about $100 per passenger in the benchmark instances. There is no significant change in the mean user costs (benchmark vs. large instance). As the number of nodes in the system increases, the biggest improvement is observed in the emission costs. More than 5-fold decrease in the average emission cost can be observed from about $5 in benchmark instances to less than 1$ in large instances.

Both the average operator cost, and average emission cost have more than halved from benchmark instances to the large instances. This is because more transit and service station nodes are used in large instances, implying better choices of transit and service station nodes for the passengers. Establishing more transit and service station nodes thus results in reduced operating costs. The best solution frontiers derived from F3E-MOGA for the large instances presented in Fig. 13 demonstrate a wide range of solutions.

F3E-MOGA is implemented in MATLAB on a Windows computer powered by AMD Ryzen 5 3550H, 16 GB RAM. Based on the benchmarking instances, the mean and standard deviations of solution convergence time per passenger are 13.32 s and 2.85 s, respectively. For the larger instances, the mean and standard deviations of solution convergence time per passenger are 12.37 s and 1.73 s, respectively. Even for the large magnitude of Ω in the larger instances, the mean convergence time per passenger remained similar. This aspect highlights the effectiveness of F3E-MOGA.

7. Summary and conclusions

Multi-echelon transportation systems are common yet highly complex to optimize. The study envisioned an integrated transit system to encourage public transit usage, offering door-to-door service through Autonomous Demand-Responsive Transit Vehicles (AuDRTVs) and promoting more sustainable travel via PuT. Fuzzy inference systems are integrated with a nondominated sorting EA. A novel concept called 'Neighborhood Score' is introduced to evaluate and enhance the quality of evolving solutions. We have developed four random genetic operators and thirteen fuzzy-guided genetic operators. Model parameters are simultaneously calibrated using Taguchi's design of experiment approach, ensuring superior convergence. The solutions obtained from the developed algorithm (F3E-MOGA) are compared with the optimal solutions. Benchmarking F3E-MOGA confirms the estimation of high-quality routing solutions, which closely approximate the Pareto optimal frontier and are well-distributed along it.

Optimizing real-world applications such as multimodal transportation systems and logistics supply chains can be computationally challenging, with multi-echelon systems being seldom studied. Existing solution methodologies often struggle to address such extensive problems. However, F3E-MOGA demonstrates capability in solving such complex problems.

Analysis of the solutions from the large problem instances revealed a reduction in operator costs per passenger, highlighting the advantages of establishing numerous transit and service station nodes. Implementing a policy of establishing multiple PuT nodes may seem costly, but counterintuitively, the results show a significant decline in the average operator cost per user, making it advantageous. Additionally, the best solution frontier demonstrates a wide range across all objectives, indicating effective solution distribution.

The system architecture has a few shortcomings. It assumes (i) every

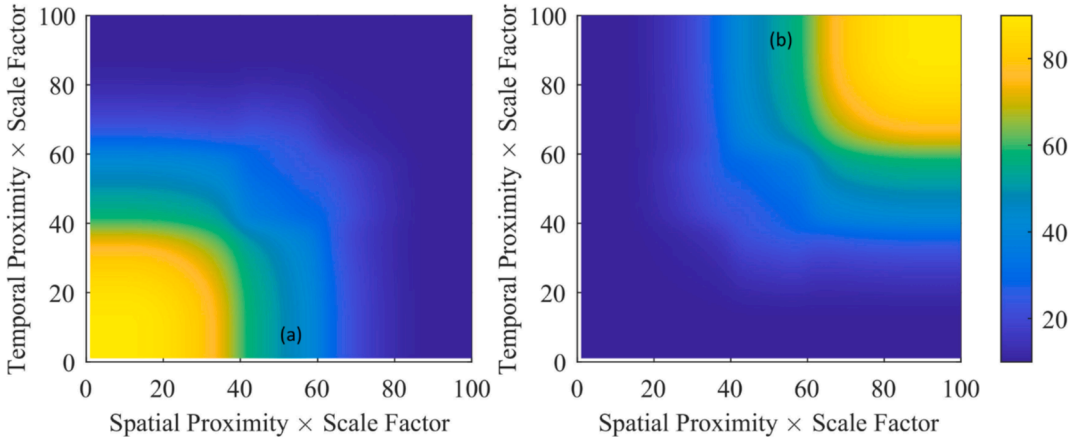

Fig. 11. NS when (a): smaller separation is better; (b): larger separation is better.

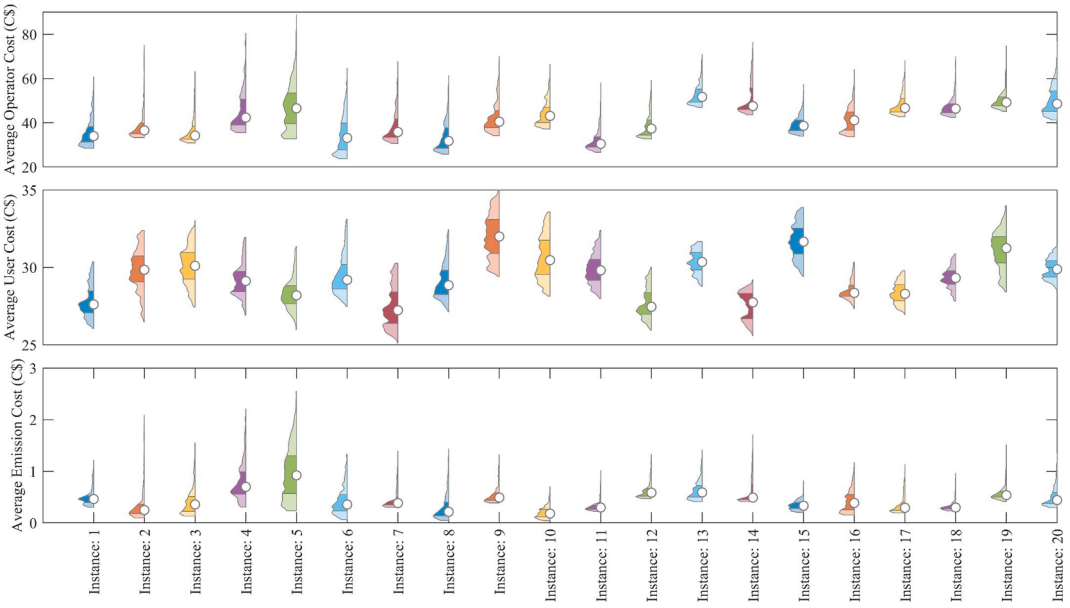

Fig. 12. Cost distribution of large validation instances solved by F3E-MOGA.

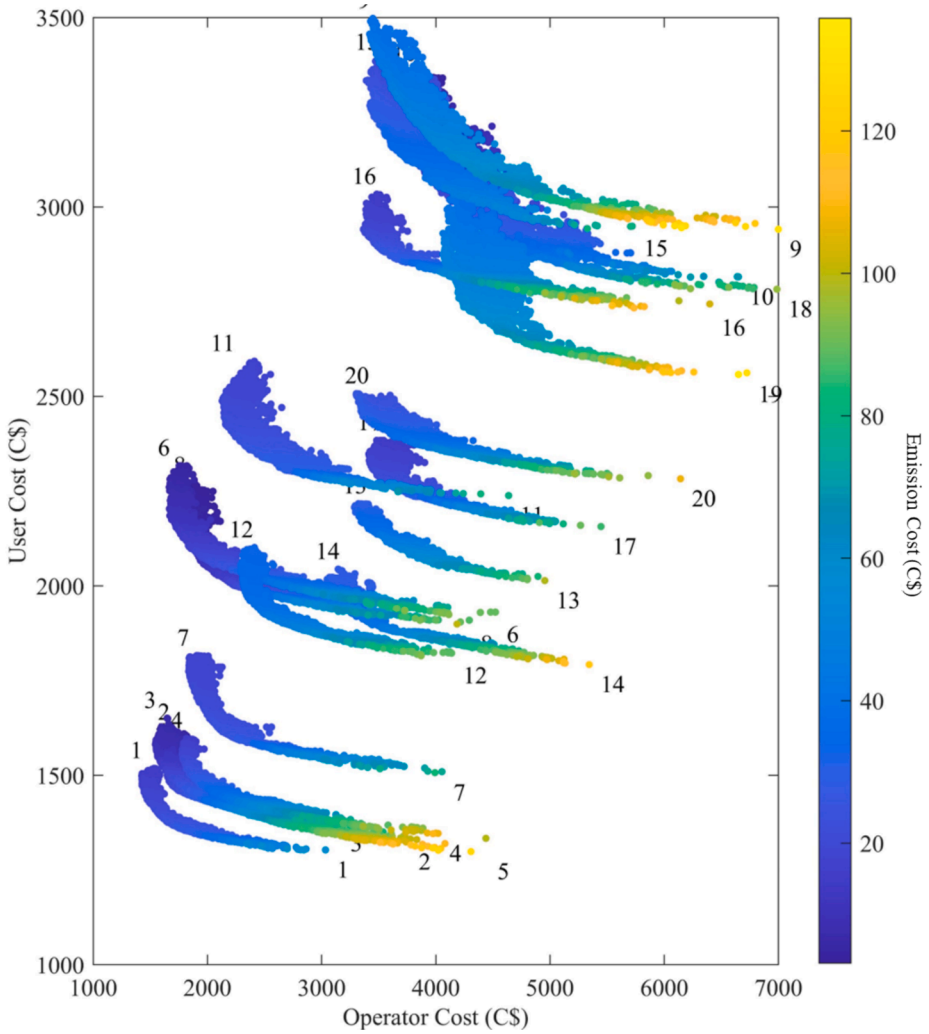

Fig. 13. Solution frontier after solving 20 large instances using F3E-MOGA.

passenger makes three legs of travel, (ii) AuDRTVs start and terminate their trips at a service station, (iii) no ride-sharing in the first and the third echelons, and (iv) the costs of waiting at the transit nodes and transfers are insignificant. All of these limitations can be addressed in future studies. Further, artificial intelligence has the potential to provide precise direction in genetic operations, replacing fuzzy-guidance. Various metaheuristic algorithms can be devised to address the optimization problem involving three echelons, followed by a comparative analysis.

Funding and acknowledgment

The authors thank the UK Research and Innovation (UKRI), and Natural Sciences and Engineering Research Council of Canada (NSERC) for funding this study (Grant Number: ALLRP 548594–2019).

CRediT authorship contribution statement

Mysore Narasimhamurthy Sharath: Writing – review & editing, Writing – original draft, Visualization, Validation, Software, Methodology, Investigation, Formal analysis, Data curation, Conceptualization. **Babak Mehran:** Writing – review & editing, Writing – original draft, Supervision, Methodology, Funding acquisition, Conceptualization. **Ahmed Ashraf:** Writing – review & editing, Writing – original draft, Conceptualization. **Susan Grant-Muller:** Writing – review & editing, Writing – original draft, Conceptualization. **Ed Manley:** Writing – review & editing, Writing – original draft, Methodology, Conceptualization.

Declaration of competing interest

The authors declare that they have no known competing financial interests or personal relationships that could have appeared to influence the work reported in this paper.

Acknowledgement

None

Annexure A: Generation of benchmarking instances

Data used and benchmarking

The multi-objective 3-echelon system used in this study is novel. As far as we know, no available instances could be used for benchmarking. Hence, several instances (with different network complexities) are developed, the procedure of which is described in this Section.

Instance generation

The number and Locations of service stations, PuT nodes, passenger travel demand, and travel costs (time and distance between any two node pairs) are the basic details necessary before generating route solutions for the passengers. A systematic procedure is adopted to generate instances. The city of Winnipeg, Canada, inspires the characteristics of generated instances. Every node $\subset\mathbb{N}$ in an instance is assumed to be confined by a square of side 20 km.

Distribution of nodes

The locations (in the cartesian plane) of transit nodes ($\mathbb{T}$) in Winnipeg are enclosed in a 20 km square. Such locations are observed to be normally distributed with.

$$\mu_X = 12,574m,\ \mu_Y = 13,131m,\ and\ \sigma^2_{XY} = \begin{bmatrix} 24316563 & 2568510 \\ 2568510 & 24902444 \end{bmatrix} m^2$$

where, μ_X, μ_Y are the mean Easting and Northing coordinates of the Winnipeg transit bus stops, and σ^2_{XY} is its covariance. Hence, the PuT nodes of $\mathbb{R}$ in the synthesized instances are assumed to be normally distributed with these properties.

A uniform distribution of Passenger Origins, $\mathbb{P}$, Destinations, $\mathbb{D}$, and Service Stations, $\mathbb{S}$, within the square bounds is assumed for every instance.

Travel cost matrices

After generating $\mathbb{N}$, the travel cost between every node pair is required. If $|\mathbb{N}| = n$, then the dimension of the cost matrix would be $n \times n$. In reality, the travel cost matrix is obtained from different sources for the chosen period. Two travel cost matrices (distance and time) are synthesized in this study.

The travel distance matrix is simply obtained by determining the Euclidean distance between the node pairs $\subset\mathbb{N}$. The Euclidean distances are rounded off to the nearest 100 m. Travel speeds by DSTVs and PuT would be different. Travel speeds in the first and third echelons are assumed to be normally distributed with a mean of 40 km/h, while that in the second echelon (PuT) are normally distributed with a mean speed of 20 km/h. The standard deviation of speeds in both cases is taken as 4 km/h. The travel time matrix is computed as the ratio between distance and speed.

From the above exercise, the spatial distribution of nodes in $\mathbb{S}, \mathbb{R}, \mathbb{C},$ and$\mathbb{D}$ is known. Subsequently, travel cost matrices are synthesized. The set of nodes, $\mathbb{N}$, and corresponding travel cost matrices form a problem instance where several passenger demands are to be served. Figure A1 depicts these nodes $\mathbb{N}$, overlayed on the map of Winnipeg.

31 problem instances are synthesized in this study. Determining the optimal solution frontier for a 3-echelon 2-objective routing problem is not trivial. It requires computing operator, user and emission costs of all the possible routes and then determining the optimal non-dominated frontier. Based on the 3-echelon architecture described earlier, the number of unique routing solutions possible is, $\Omega \approx |\mathbb{S}| \times |\mathbb{P}| \times |\mathbb{R}| \times |\mathbb{S}| \times |\mathbb{S}| \times |\mathbb{R}| \times |\mathbb{S}|$. Even for a small instance containing 10 passenger nodes, 10 service station nodes, and 10 PuT nodes, approximately 10^7 (10 million) unique routing solutions are possible. Thus, it is computationally impossible to obtain an optimal solution for larger and more realistic instances by exhaustive exploration. However, Pareto optimal solutions are necessary to assess the quality of solutions obtained from F3E-MOGA. Thus, the exhaustive exploration technique is adopted to optimally solve 11 problem instances (11 benchmarking instances). The remaining 20 problem instances are large instances.

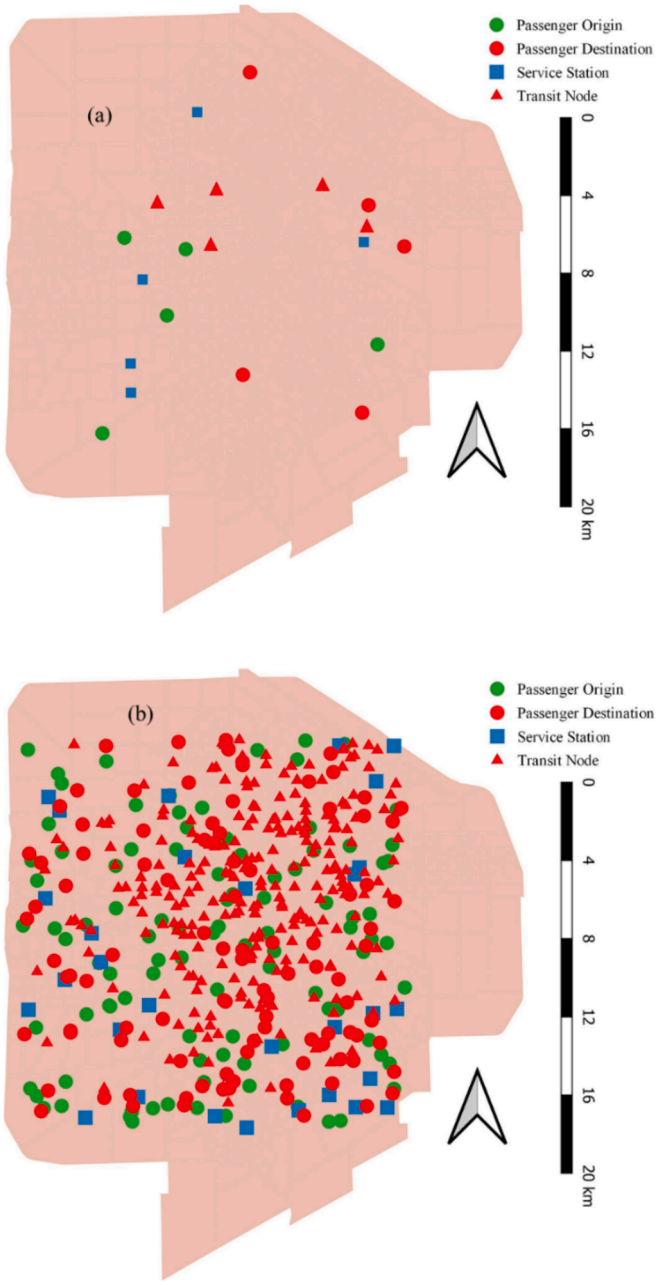

Fig. A1. (a) a benchmark instance with ; (b) a large instance with

Annexure B: Random genetic operations

Fuzzy-guided operators may result in a solution getting stuck at a locally optimal point. Random genetic operations in an EA are necessary to release the solutions from local optima. It is required to develop random genetic operations tailored for the present study. Four such genetic operators are custom-built in this study. The probability of each of these genetic operations is a parameter to be calibrated. The process of calibration and the calibrated parameters are presented in Section 4.1 and Section 5, respectively.

Service station crossover operator (SSX)

Fig B.1(a) portrays the SSX operation involving two parents. A service station gene in a stack of chromosomes is randomly selected from both parents. These two genes are then swapped, resulting in two offsprings. A similar genetic operation is possible with one parent resulting in one offspring. Both the asexual and sexual crossover operations are assumed equally probable. The probability of SSX operation is p_{SSX}.

Passenger route crossover operator (PasRX)

Fig B.1(b) shows the PasRX operation involving two parents. An entire chromosome from a stack of chromosomes is randomly chosen from a parent. The passenger being served is then noted. The chromosome for the same passenger from another parent is then selected. These two chromosomes are then swapped between the two parents resulting in two offsprings. The probability of PasRX operation is p_{PasRX}.

Transit node crossover operator (TNX)

As the name suggests, a transit node gene is randomly chosen from two parents. The two genes are then swapped, resulting in two offsprings. Such an operation can also be performed with only a single parent resulting in one offspring. The probability of both the sexual and asexual TNX operation is considered equally likely and is $p_{TNX.}$ See Fig. B.1(c).

Partial route crossover operator (ParRX)

The genes 1 to 4 of a chromosome represent the route of AuDRTV-1, while genes 5 to 8 correspond to the route of AuDRTV-2. Route of AuDRTV-1 or AuDRTV-2 of one of the passengers is randomly selected, and the corresponding passenger is noted in ParRX operation. The route of AuDRTV-1 or AuDRTV-2 for the same passenger from another parent is selected. These partial routes are then swapped. The probability of ParRX operation is p_{ParRX}. See Fig B.1(d).

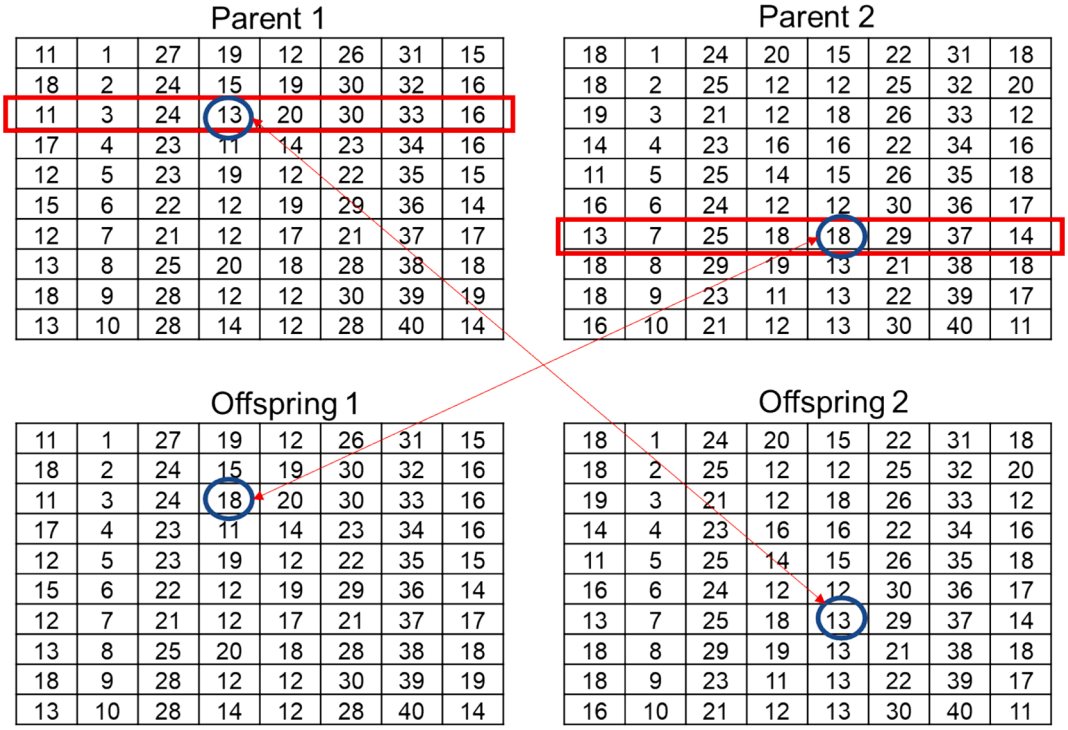

Fig. B1a. Service Station Crossover Operation

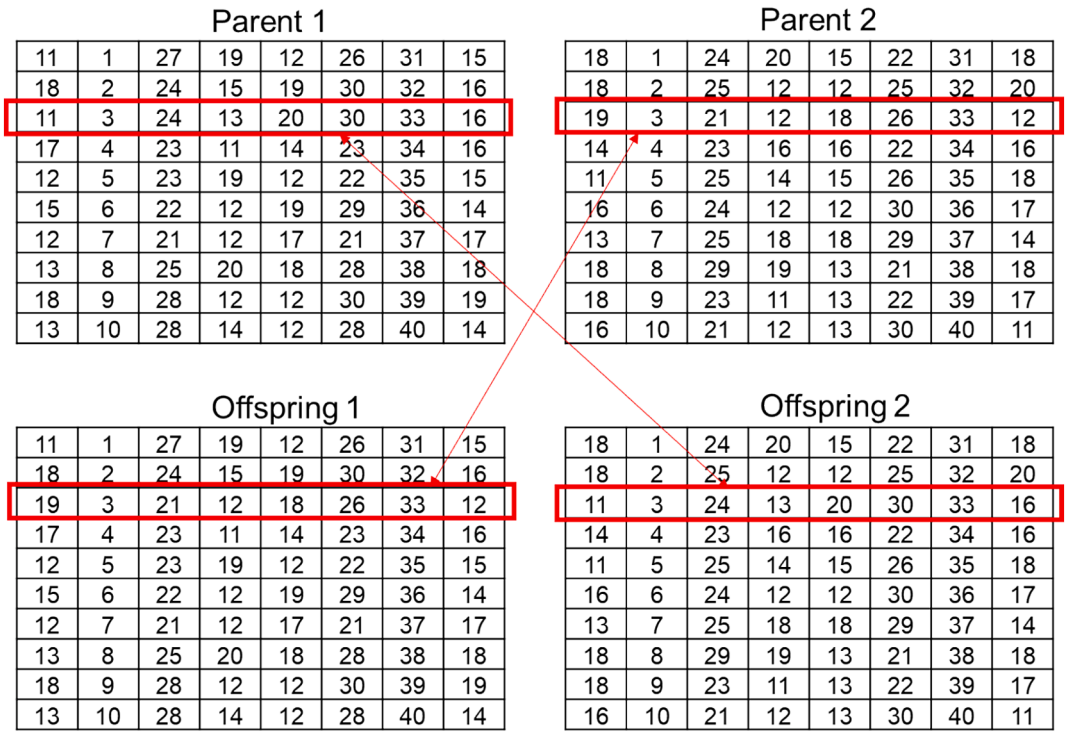

Fig. B1b. Passenger Route Crossover Operation

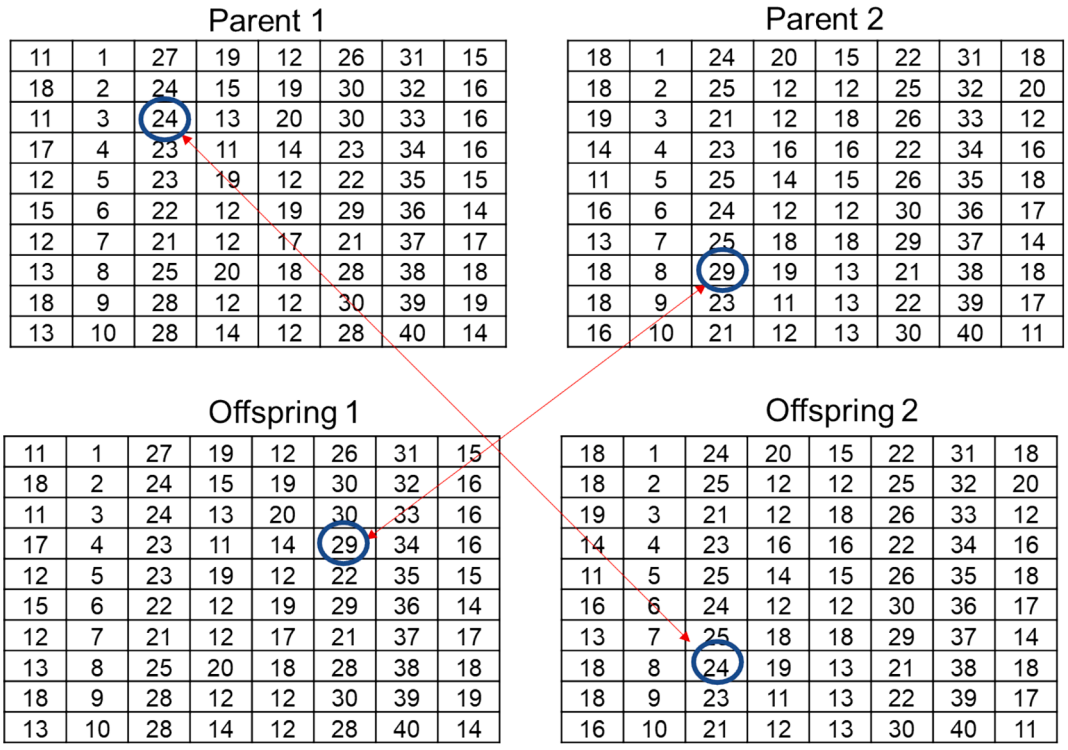

Fig. B1c. Transit Node Crossover Operation

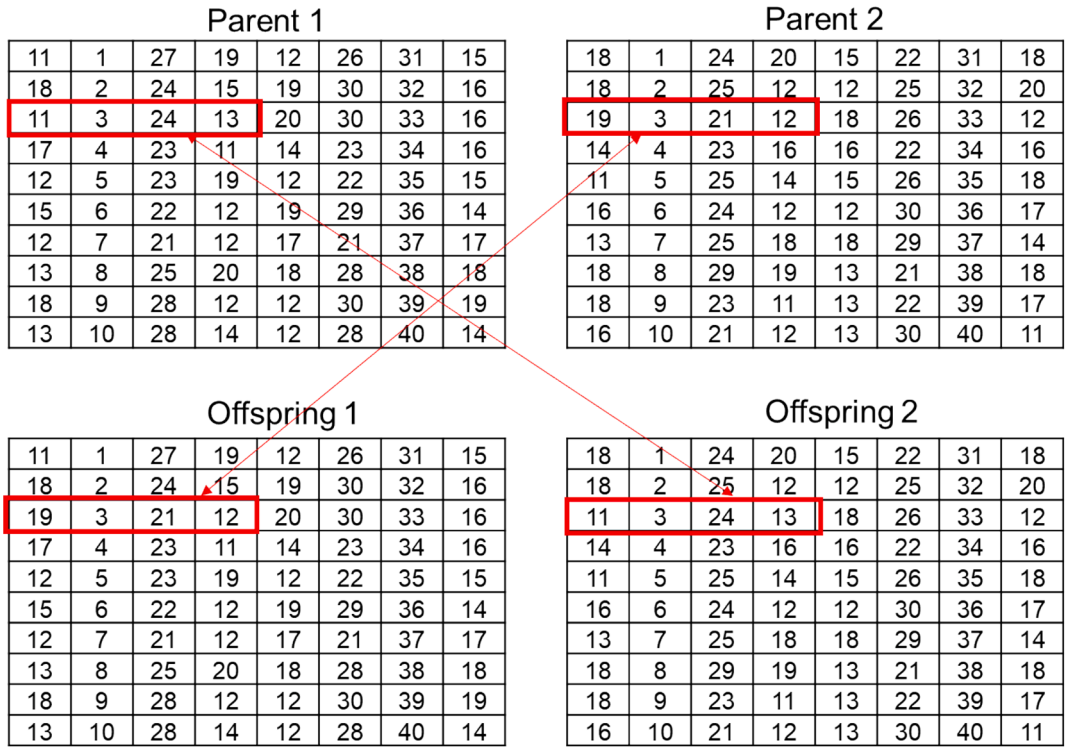

Fig. B1d. Partial Route Crossover Operation

Annexure C: Evolutionary algorithm

Initial random population

The EA is initiated with randomly generated members. A member is represented as a matrix of dimension $|\mathbb{P}| \times 8$, where $|\mathbb{P}|$ is the cardinality of $\mathbb{P}$. Columns 1 and 5 are filled up from set $\mathbb{S}$ (random sampling without replacement). Elements of columns 4 and 8 are randomly sampled from $\mathbb{SS}$ (with replacement). Columns 3 and 6 are filled with elements from $\mathbb{R}$ (random sampling with replacement). Columns 2 and 7 correspond to the origin and destination of the passengers, which are obtained from $\mathbb{P}$ and $\mathbb{D}$. Please refer to Table 1 for the description of the notations used.

The above is the procedure for generating random routing solutions for all passengers (or a member). Such solutions satisfy all the constraints mentioned in Section 3.2. Several such members are generated to form the initial random population. A large population would be a computation burden, while a small population would result in insufficient exploration. Population size is one of the crucial parameters and thus has been calibrated.

Fitness evaluation of the members

The offsprings and the parents from every generation are pooled before evaluating their fitness. This is a commonly adopted elite preservation strategy. When the fitness of every member of the pooled population is evaluated, the fitter parents or offsprings survive for future generations. A member's fitness is evaluated using the three objectives. The three fitness measures (C_{UC}, C_{OC}, and C_{EC}) are computed for every member of the population.

Nondominated sorting

In a multi-objective optimization problem, the concept of domination is used to identify the relative fitness of different population members. Nondominated sorting (as described in Deb et al. (2002)) is performed to determine the nondominated frontiers (or sets). The best nondominated frontier is $\mathscr{F}_1$, followed by $\mathscr{F}_2$, $\mathscr{F}_3$, and so on.

Population diversity control and niching

If the population from one generation is pooled with the offsprings, the population size for the next generation will increase. Some of the weaker (frequently dominated) members are to be excluded from future generations for a fixed population size. In doing so, the diversity of the population is to be preserved. Preserving population diversity is one of the significant challenges in EAs (Li et al., 2017). This study uses a Hypervolume indicator provided in Equation (12) as a population diversity indicator.

$$\mathscr{H}_k = \mathbb{d}_{k,UC} \times \mathbb{d}_{k,OC} \times \mathbb{d}_{k,EC} \tag{12}$$

$$\mathbb{d}_{k,UC} = C_{k,UC} - C_{UC}^{Reference} \tag{13a}$$

$$\mathbb{d}_{k,OC} = C_{k,OC} - C_{OC}^{Reference} \tag{13b}$$

$$\mathbb{d}_{k,EC} = C_{k,EC} - C_{EC}^{Reference} \tag{13c}$$

where, $\mathscr{H}_i$ is the hypervolume indicator of member k;

$\mathbb{d}_{k,UC}$ is the distance (from an arbitrary but fixed reference point) of member k in user costs;

$\mathbb{d}_{k,OC}$ is the distance of member k in operator costs;

$\mathbb{d}_{k,EC}$ is the distance of member k in emission costs;

$C_{UC}^{Reference} = 0$, $C_{OC}^{Reference} = 0$, and $C_{EC}^{Reference} = 0$, are the three fixed reference points used in this study; and $C_{k,UC}, C_{k,OC}$, and $C_{k,EC}$ respectively are the user cost, operator cost and emission cost associated with member k.

Frontiers $\mathscr{F}_1, \mathscr{F}_2, \cdots \mathscr{F}_{n-1}$ from the parent-offspring pool survive for the future generations if $|\mathscr{F}_1| + |\mathscr{F}_2| + \cdots + |\mathscr{F}_{n-1}| \leq \mathscr{N}$, where $\mathscr{N}$ is the desired population size. The remaining k members ($k = \mathscr{N} - [|\mathscr{F}_1| + |\mathscr{F}_2| + \cdots + |\mathscr{F}_{n-1}|]$) are obtained from nondominated frontier $\mathscr{F}_n$. The process of selecting members from nondominated frontier $\mathscr{F}_n$ is called Niching. In this study, k members are selected using k-means clustering strategy. Hypervolume indicator, $\mathscr{H}$ of the members of the frontier $\mathscr{F}_n$ are used to form k clusters. The best member (with smallest $\mathscr{H}$) from each cluster is then selected for future generations. Such a clustering technique ensures population diversity. The number of nondominated frontiers reduces, and the number of members in the first frontier increases as members evolve. It is then the effect of niching becomes prominent and essential.

Selection of members for evolution

2-way tournament selection and fitness proportionate selection strategies are randomly used (with equal probability) to select the members (parents) to perform genetic operations.

Solution convergence criteria

Let $\mathscr{g}$ be the number of generations for which evolution is permitted and, $\mathscr{H}^{\mathscr{g}}_{best}$ be the hypervolume indicator of the best (lowest magnitude) member at generation $\mathscr{g}$. The solution is said to be converged if $(\mathscr{H}^{\mathscr{g}-300}_{best} - \mathscr{H}^{\mathscr{g}}_{best})/\mathscr{H}^{\mathscr{g}}_{best} < 0.01$. That is, if the $\mathscr{H}$ does not improve by more than 1 % in successive 300 generations, the solution is said to be converged. The bounds for the number of generations in this study are $300 \leq \mathscr{g} \leq 30000$.

Annexure D: Benchmarking

Table D1 and Table D2 provide characteristics of benchmarking and large instances respectively.

Table D1
Characteristics of benchmarking instances.

Instance ID	$\lvert\mathbb{P}\rvert$	$\lvert\mathbb{S}\rvert$	$\lvert\mathbb{R}\rvert$	$\lvert\mathbb{N}\rvert$	$\Omega(\times 10^6)$
1	5	5	5	20	0.078125
2	10	5	5	30	0.15625
3	5	5	10	25	0.3125
4	5	5	15	30	0.703125
5	5	10	5	25	1.25
6	5	5	20	35	1.25
7	5	5	25	40	1.953125
8	5	5	30	45	2.8125
9	5	5	35	50	3.828125
10	5	5	40	55	5
11	5	10	10	30	5

Table D2
Characteristics of large instances dataset.

Instance ID	$\|\mathbb{P}\|$	$\|\mathbb{S}\|$	$\|\mathbb{R}\|$	$\|\mathbb{N}\|$	$\Omega(\times 10^9)$	Convergence time (s)
1	50	20	300	420	720.0	661.7
2	50	15	250	365	158.2	519.3
3	50	10	200	310	20.0	686.5
4	50	15	150	265	57.0	738.2
5	50	15	100	215	25.3	608.7
6	70	25	100	265	273.4	982.6
7	60	20	250	390	600.0	821.7
8	70	15	250	405	221.5	1051.8
9	100	30	100	330	810.0	1291.3
10	100	30	250	480	5062.5	1122.4
11	80	30	200	390	2592.0	1203.1
12	70	20	100	260	112.0	823.8
13	70	10	50	200	1.8	625.1
14	70	10	100	250	7.0	848.8
15	100	10	100	310	10.0	1048.4
16	100	15	250	465	316.4	1294.4
17	80	10	300	470	72.0	995.7
18	100	10	300	510	90.0	1164.7
19	90	15	50	245	11.4	980.3
20	80	20	100	280	128.0	805.1

$|\mathbb{P}|$: Number of passenger origin nodes.
$|\mathbb{D}|$: Number of passenger destination nodes.
$|\mathbb{S}|$: Number of service station nodes.
$|\mathbb{R}|$: Number of PuT nodes.
$|\mathbb{N}|$: Total number of nodes.
Ω: Total number of routing solutions possible.

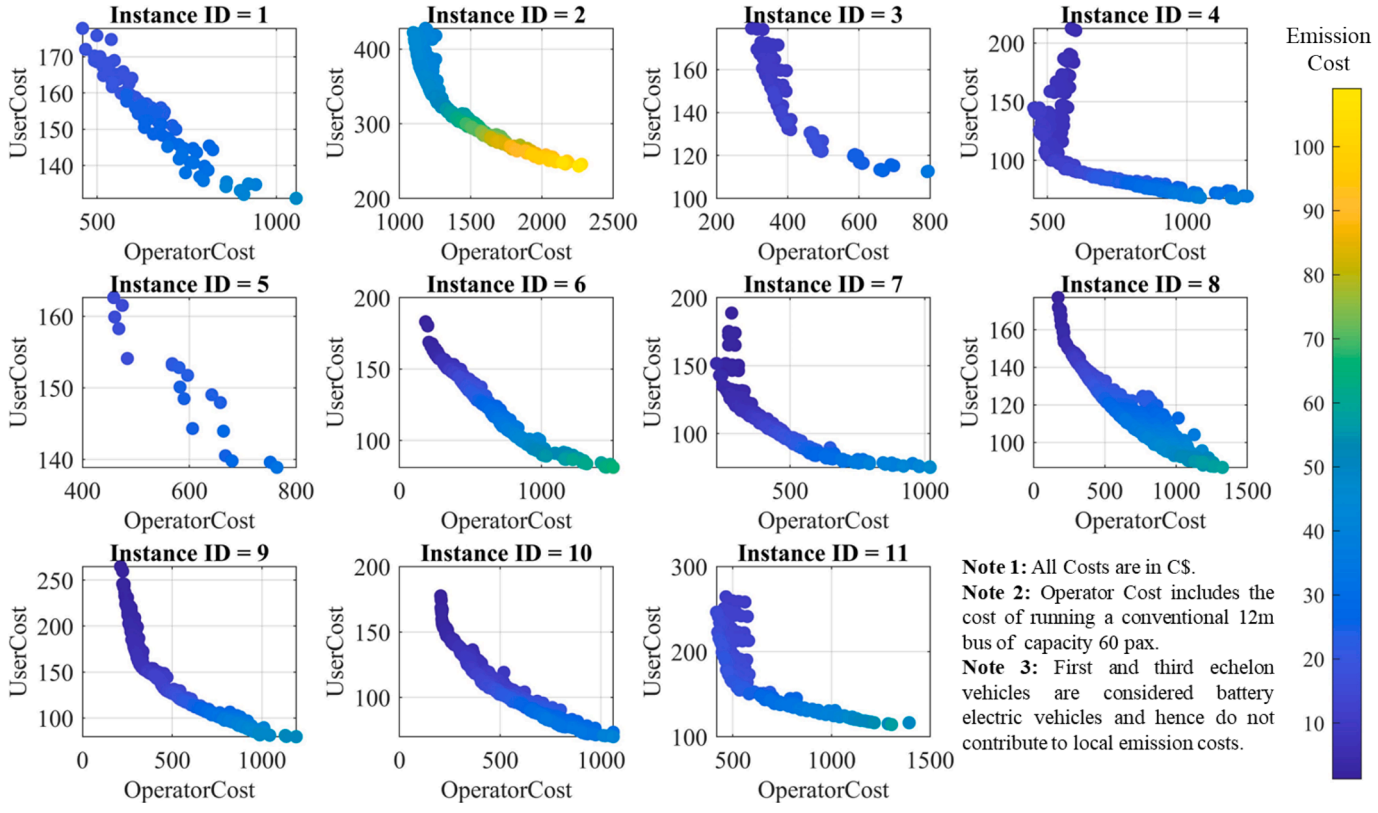

Fig. D1a. Optimal frontiers of benchmark instances, determined by exploring all possible solutions

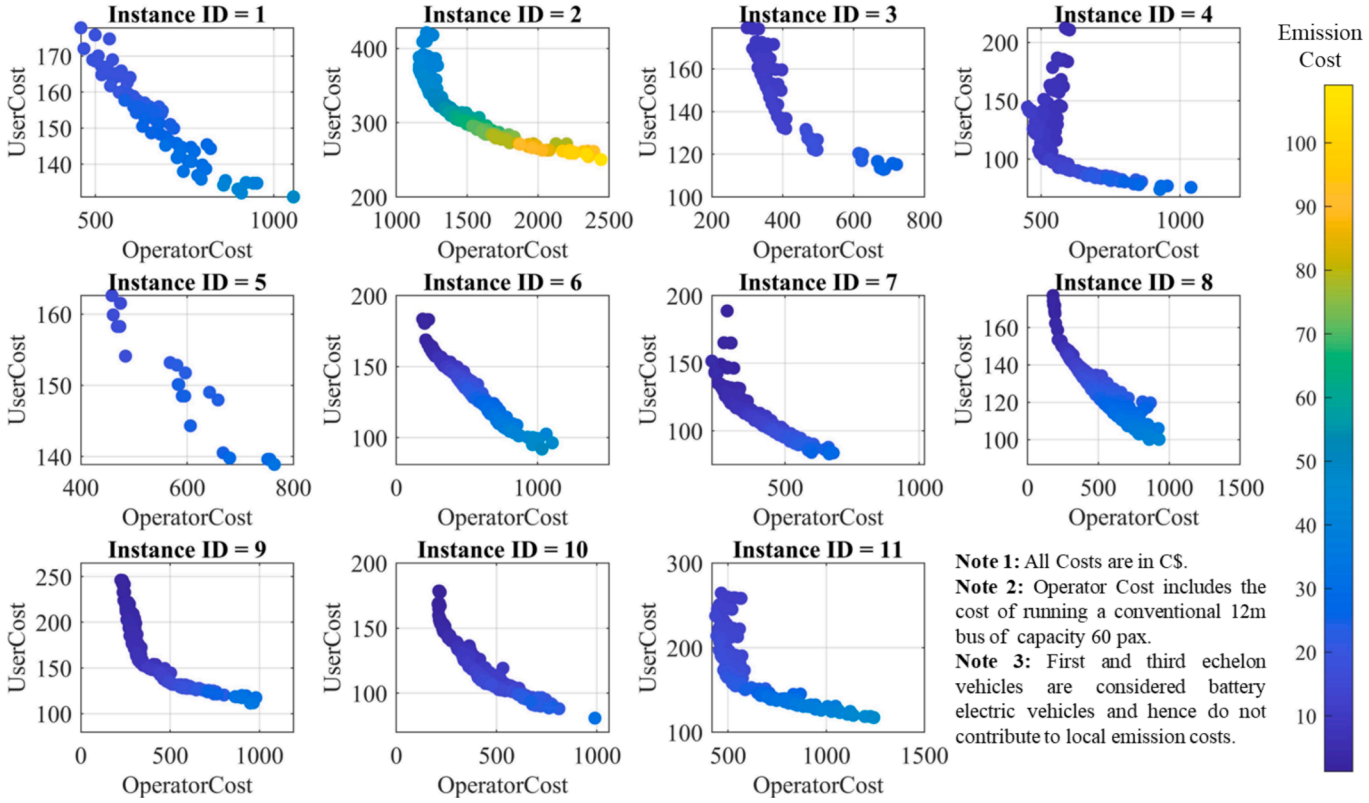

Fig. D1b. Best frontier determined by F3EMOGA after solving benchmark instances

It can be observed that the best frontier of F3E-MOGA is very close to the Pareto optimal frontier. Also, F3E-MOGA solutions are well distributed along the Pareto optimal frontier.

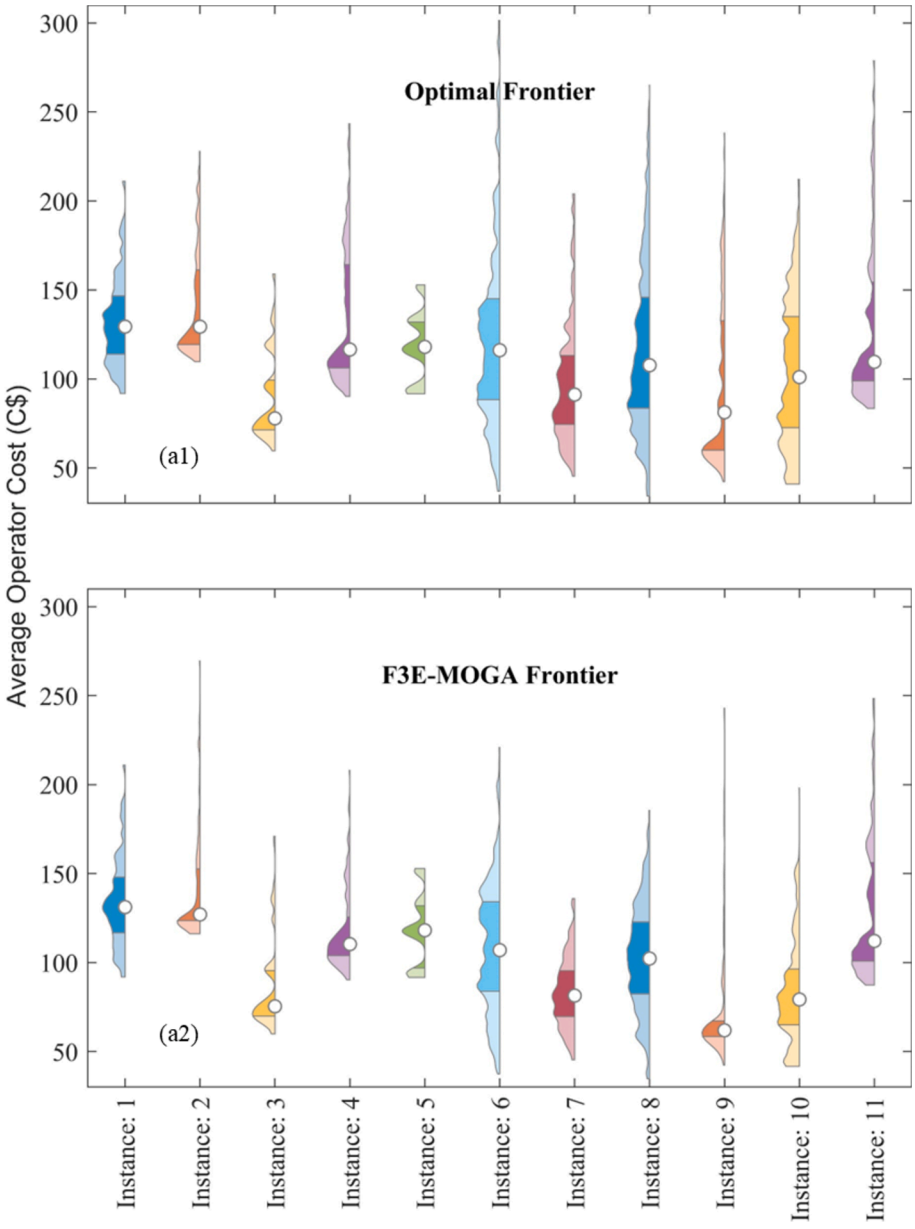

Fig. D2a. Distribution of average operator costs per user in the best frontier of benchmark instances

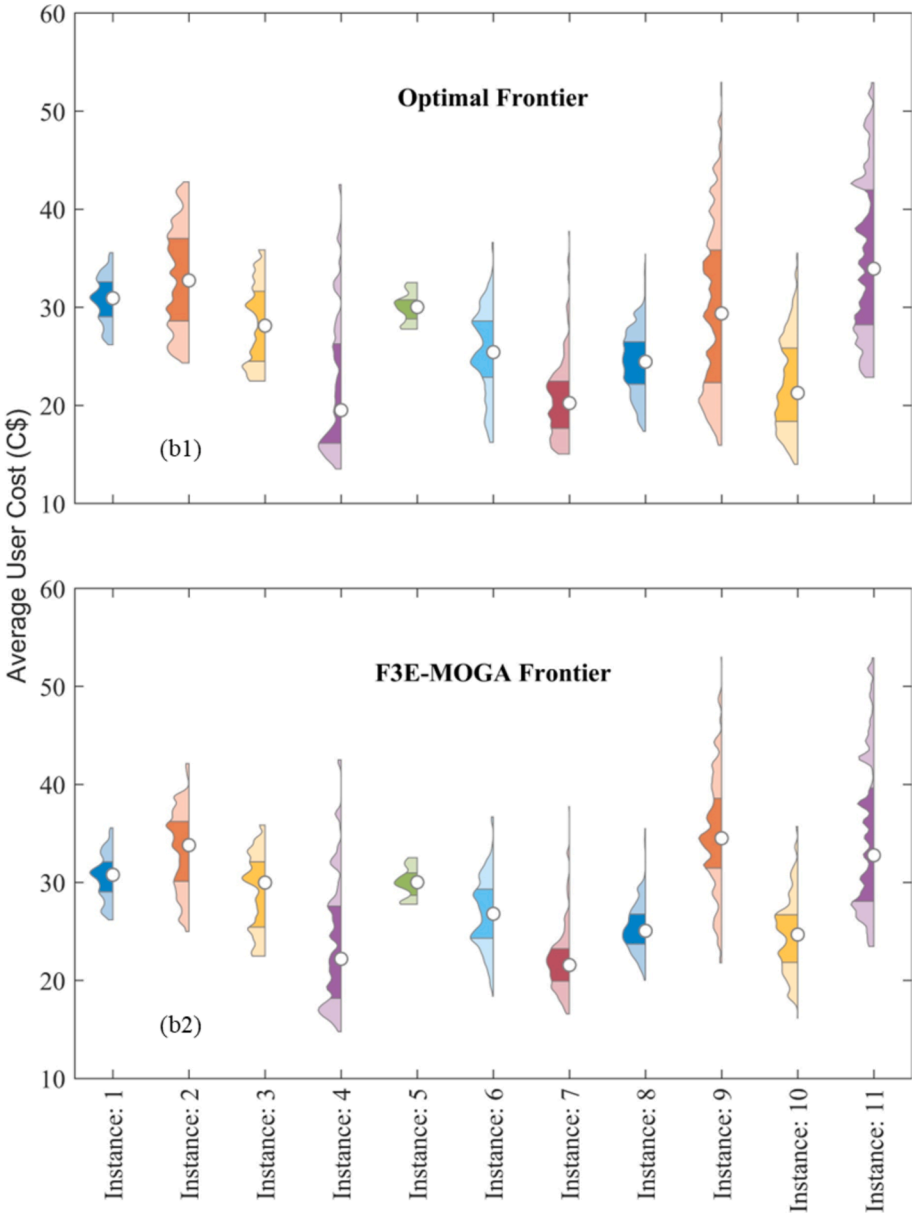

Fig. D2b. Distribution of average user costs per user in the best frontier of benchmark instances

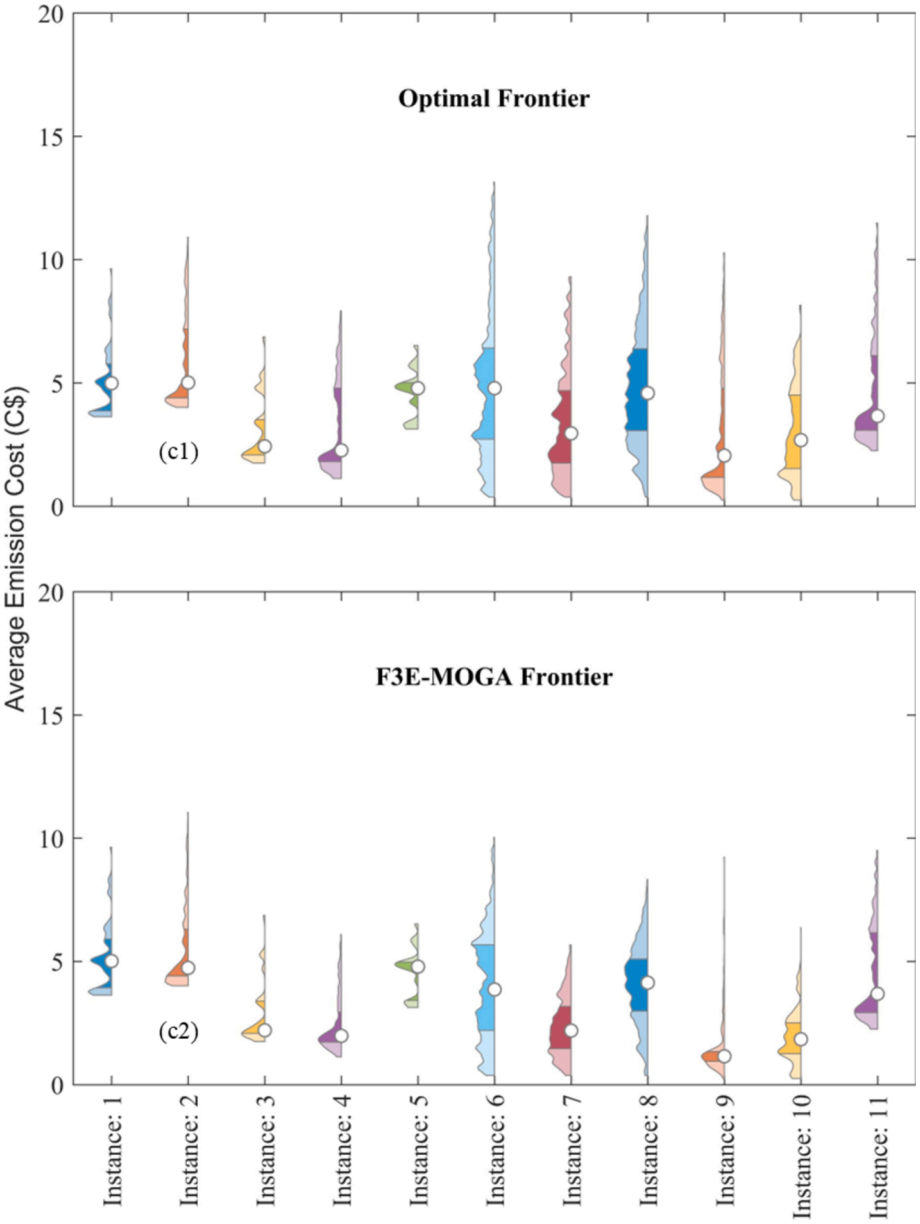

Fig. D2c. Distribution of average emission costs per user in the best frontier of benchmark instances

Data availability

Data will be made available on request.

References

Abhang, L.B., Hameedullah, M., 2012. Determination of optimum parameters for multi-performance characteristics in turning by using grey relational analysis. Int. J. Adv. Manuf. Technol. 63, 13–24. https://doi.org/10.1007/s00170-011-3857-6.

Agárdi, A., Kovács, L., Bányai, T., 2021. An attraction map framework of a complex multi-echelon vehicle routing problem with random walk analysis. Appl. Sci. 11, 2100. https://doi.org/10.3390/app11052100.

Agatz, N., Erera, A., Savelsbergh, M., Wang, X., 2012. Optimization for dynamic ride-sharing: A review. Eur. J. Oper. Res. 223, 295–303. https://doi.org/10.1016/j.ejor.2012.05.028.

Aiko, S., Thaithatkul, P., Asakura, Y., 2018. Incorporating user preference into optimal vehicle routing problem of integrated sharing transport system. Asian Transport Stud. 5, 98–116. https://doi.org/10.11175/eastsats.5.98.

Alogdianakis, F., Dimitriou, L., 2023. Optimal mechanism design of public policies for promoting electromobility: A dynamic programming formulation. Transp. Res. Interdiscip. Perspect. 19, 100807. https://doi.org/10.1016/j.trip.2023.100807.

Aloui, A., Hamani, N., Derrouiche, R., Delahoche, L., 2021. Systematic literature review on collaborative sustainable transportation: overview, analysis and perspectives. Transp. Res. Interdiscip. Perspect. 9, 100291. https://doi.org/10.1016/j.trip.2020.100291.

Barraza, O., Estrada, M., 2021. Battery electric bus network: efficient design and cost comparison of different powertrains. Sustainability 13, 4745. https://doi.org/10.3390/su13094745.

Beheshtinia, M.A., Salmabadi, N., Rahimi, S., 2021. A robust possibilistic programming model for production-routing problem in a three-echelon supply chain. J. Model. Manag. 16, 1328–1357. https://doi.org/10.1108/JM2-06-2020-0162.

Belgin, O., Karaoglan, I., Altiparmak, F., 2018. Two-echelon vehicle routing problem with simultaneous pickup and delivery: Mathematical model and heuristic approach. Comput. Ind. Eng. 115, 1–16. https://doi.org/10.1016/j.cie.2017.10.032.

Braekers, K., Ramaekers, K., Van Nieuwenhuyse, I., 2016. The vehicle routing problem: State of the art classification and review. Comput. Ind. Eng. 99, 300–313. https://doi.org/10.1016/j.cie.2015.12.007.

Cao, E., Lai, M., 2010. The open vehicle routing problem with fuzzy demands. Expert Syst. Appl. 37, 2405–2411. https://doi.org/10.1016/j.eswa.2009.07.021.

Coindreau, M.-A., Gallay, O., Zufferey, N., 2019. Vehicle routing with transportable resources: using carpooling and walking for on-site services. Eur. J. Oper. Res. 279, 996–1010. https://doi.org/10.1016/j.ejor.2019.06.039.

Davis, M., Ahiduzzaman, Md., Kumar, A., 2018. How will Canada's greenhouse gas emissions change by 2050? A disaggregated analysis of past and future greenhouse gas emissions using bottom-up energy modelling and Sankey diagrams. Appl. Energy 220, 754–786. https://doi.org/10.1016/j.apenergy.2018.03.064.

Deb, K., Pratap, A., Agarwal, S., Meyarivan, T., 2002. A fast and elitist multiobjective genetic algorithm: NSGA-II. IEEE Trans. Evol. Comput. 6, 182–197. https://doi.org/10.1109/4235.996017.

Dellaert, N., Dashty Saridarq, F., Van Woensel, T., Crainic, T.G., 2019. Branch-and-price–based algorithms for the two-echelon vehicle routing problem with time windows. Transp. Sci. 53, 463–479. https://doi.org/10.1287/trsc.2018.0844.

Díaz-Parra, O., Ruiz-Vanoye, J.A., Bernábe Loranca, B., Fuentes-Penna, A., Barrera-Cámara, R.A., 2014. A survey of transportation problems. J. Appl. Math. 2014, 1–17. https://doi.org/10.1155/2014/848129.

Dimatulac, T., Maoh, H., Carriveau, R., 2023. An archetypal routing network model to help identify potential charging locations for long-haul electric vehicles in Ontario, Canada. Transportation Research Interdisciplinary Perspectives 19, 100825. https://doi.org/10.1016/j.trip.2023.100825.

Elshaer, R., Awad, H., 2020. A taxonomic review of metaheuristic algorithms for solving the vehicle routing problem and its variants. Comput. Ind. Eng. 140, 106242. https://doi.org/10.1016/j.cie.2019.106242.

Farajzadeh, F., Moadab, A., Valilai, O.F., Houshmand, M., 2020. A novel mathematical model for a cloud-based drone enabled vehicle routing problem considering multi-echelon supply chain. IFAC-PapersOnLine 53, 15035–15040. https://doi.org/10.1016/j.ifacol.2020.12.2004.

Feng, H.-M., Liao, K.-L., 2014. Hybrid evolutionary fuzzy learning scheme in the applications of traveling salesman problems. Inf. Sci. 270, 204–225. https://doi.org/10.1016/j.ins.2014.02.098.

Gayialis, S.P., Konstantakopoulos, G.D., Tatsiopoulos, I.P., 2019. Vehicle Routing Problem for Urban Freight Transportation: A Review of the Recent Literature. Springer Science and Business Media B.V, pp. 89–104.

Ghannadpour, S.F., Noori, S., Tavakkoli-Moghaddam, R., Ghoseiri, K., 2014. A multi-objective dynamic vehicle routing problem with fuzzy time windows: Model, solution and application. Appl. Soft Comput. 14, 504–527. https://doi.org/10.1016/j.asoc.2013.08.015.

Ghannadpour, S.F., Zarrabi, A., 2019. Multi-objective heterogeneous vehicle routing and scheduling problem with energy minimizing. Swarm Evol. Comput. 44, 728–747. https://doi.org/10.1016/j.swevo.2018.08.012.

Guo, R., Guan, W., Zhang, W., Meng, F., Zhang, Z., 2019. Customized bus routing problem with time window restrictions: model and case study. Transportmetrica A: Transport Science 15, 1804–1824. https://doi.org/10.1080/23249935.2019.1644566.

Guo, X., Zhang, W., Liu, B., 2022. Low-carbon routing for cold-chain logistics considering the time-dependent effects of traffic congestion. Transp. Res. Part D: Transp. Environ. 113, 103502. https://doi.org/10.1016/j.trd.2022.103502.

Hulagu, S., Celikoglu, H.B., 2022. An Electric Vehicle Routing Problem With Intermediate Nodes for Shuttle Fleets. IEEE Trans. Intell. Transp. Syst. 23, 1223–1235. https://doi.org/10.1109/TITS.2020.3023673.

Kabir, M., Mobin, J., Nayeem, M.A., Habib, M.A., Rahman, M.S., 2023. Multi-objective optimization and heuristic based solutions for evacuation modeling. Transp. Res. Interdiscip. Perspect. 18, 100798. https://doi.org/10.1016/j.trip.2023.100798.

Konstantakopoulos, G.D., Gayialis, S.P., Kechagias, E.P., 2020. Vehicle routing problem and related algorithms for logistics distribution: a literature review and classification. Oper. Res. https://doi.org/10.1007/s12351-020-00600-7.

Lau, H.C.W., Chan, T.M., Tsui, W.T., Chan, F.T.S., Ho, G.T.S., Choy, K.L., 2009. A fuzzy guided multi-objective evolutionary algorithm model for solving transportation problem. Expert Syst. Appl. 36, 8255–8268. https://doi.org/10.1016/j.eswa.2008.10.031.

Li, X., Epitropakis, M.G., Deb, K., Engelbrecht, A., 2017. Seeking multiple solutions: an updated survey on niching methods and their applications. IEEE Trans. Evol. Comput. 21, 518–538. https://doi.org/10.1109/TEVC.2016.2638437.

Lin, C., Choy, K.L., Ho, G.T.S., Chung, S.H., Lam, H.Y., 2014. Survey of green vehicle routing problem: past and future trends. Expert Syst. Appl. 41, 1118–1138. https://doi.org/10.1016/j.eswa.2013.07.107.

Masmoudi, M.A., Hosny, M., Koç, Ç., 2022. The fleet size and mix vehicle routing problem with synchronized visits. Transp. Lett. 14, 427–445. https://doi.org/10.1080/19427867.2021.1888196.

Mehran, B., Yang, Y., Mishra, S., 2020. Analytical models for comparing operational costs of regular bus and semi-flexible transit services. Public Transp. 12, 147–169. https://doi.org/10.1007/s12469-019-00222-z.

Nickkar, A., Lee, Y.-J., Meskar, M., 2022. Developing an optimal algorithm for demand responsive feeder transit service accommodating temporary stops. J. Public Transp. 24, 100021. https://doi.org/10.1016/j.jpubtr.2022.100021.

Parvez Farazi, N., Zou, B., Ahamed, T., Barua, L., 2021. Deep reinforcement learning in transportation research: a review. Transp. Res. Interdiscip. Perspect. 11, 100425. https://doi.org/10.1016/j.trip.2021.100425.

Querini, F., Béziat, J.-C., Morel, S., Boch, V., Rousseaux, P., 2011. Life cycle assessment of automotive fuels: critical analysis and recommendations on the emissions inventory in the tank to wheels stage. Int J Life Cycle Assess 16, 454–464. https://doi.org/10.1007/s11367-011-0273-y.

Rattanawai, N., Arunyanart, S., Pathumnakul, S., 2024. Optimizing municipal solid waste collection vehicle routing with a priority on infectious waste in a mountainous city landscape context. Transp. Res. Interdiscip. Perspect. 24, 101066. https://doi.org/10.1016/j.trip.2024.101066.

Rezaei, S., Khojandi, A., Mohsena Haque, A., Brakewood, C., Jin, M., Cherry, C.R., 2022. Park-and-ride facility location optimization: A case study for Nashville, Tennessee. Transportation Research Interdisciplinary Perspectives 13, 100578. https://doi.org/10.1016/j.trip.2022.100578.

Ritchie, H., Roser, M., Rosado, P., 2020. CO_2 and greenhouse gas emissions. Our World in Data.

Saragih, N.I., Bahagia, S.N., Suprayogi, S., I.,, 2019. A heuristic method for location-inventory-routing problem in a three-echelon supply chain system. Comput. Ind. Eng. 127, 875–886. https://doi.org/10.1016/j.cie.2018.11.026.

Sharath, M.N., Velaga, N.R., 2020. Enhanced intelligent driver model for two-dimensional motion planning in mixed traffic. Transp. Res. Part C Emerging Technol. 120, 102780. https://doi.org/10.1016/j.trc.2020.102780.

Shen, X., Guo, Y., Chen, Q., Hu, W., 2010. A multi-objective optimization evolutionary algorithm incorporating preference information based on fuzzy logic. Comput. Optim. Appl. 46, 159–188. https://doi.org/10.1007/s10589-008-9189-2.

Srivatsa Srinivas, S., Marathe, R.R., 2021. Moving towards "mobile warehouse": Last-mile logistics during COVID-19 and beyond. Transp. Res. Interdiscip. Perspect. 10, 100339. https://doi.org/10.1016/j.trip.2021.100339.

Taguchi, G., Chowdhury, S., Wu, Y., 2005. Appendix A: Orthogonal Arrays and Linear Graphs: Tools for Quality Engineering, in: Taguchi's Quality Engineering Handbook. John Wiley & Sons, Inc., Hoboken, NJ, USA, pp. 1523–1597. 10.1002/9780470258354.app1.

Thao, V.T., Imhof, S., Von Arx, W., 2021. Integration of ridesharing with public transport in rural Switzerland: Practice and outcomes. Transp. Res. Interdiscip. Perspect. 10, 100340. https://doi.org/10.1016/j.trip.2021.100340.

Tian, Y., Zhang, X., Cheng, R., Jin, Y., 2016. A multi-objective evolutionary algorithm based on an enhanced inverted generational distance metric. In: IEEE Congress on Evolutionary Computation (CEC). IEEE, pp. 5222–5229. https://doi.org/10.1109/CEC.2016.7748352.

Vidal, T., Laporte, G., Matl, P., 2020. A concise guide to existing and emerging vehicle routing problem variants. Eur. J. Oper. Res. 286, 401–416. https://doi.org/10.1016/j.ejor.2019.10.010.

Whitmore, A., Samaras, C., Hendrickson, C.T., Scott Matthews, H., Wong-Parodi, G., 2022. Integrating public transportation and shared autonomous mobility for equitable transit coverage: A cost-efficiency analysis. Transp. Res. Interdiscip. Perspect. 14, 100571. https://doi.org/10.1016/j.trip.2022.100571.

Yan, X., Huang, H., Hao, Z., Wang, J., 2020. A graph-based fuzzy evolutionary algorithm for solving two-echelon vehicle routing problems. IEEE Trans. Evol. Comput. 24, 129–141. https://doi.org/10.1109/TEVC.2019.2911736.

Ye, Z., Yu, N., Wei, R., Liu, X.C., 2022. Decarbonizing regional multi-model transportation system with shared electric charging hubs. Transp. Res. Part C Emerging Technol. 144, 103881. https://doi.org/10.1016/j.trc.2022.103881.

Zhang, L., Liu, Z., Yu, L., Fang, K., Yao, B., Yu, B., 2022. Routing optimization of shared autonomous electric vehicles under uncertain travel time and uncertain service time. Transportation Research Part e: Logistics and Transportation Review 157, 102548. https://doi.org/10.1016/j.tre.2021.102548.